

RS-02-122

July 19, 2002

U. S. Nuclear Regulatory Commission
ATTN: Document Control Desk
Washington, D C 20555

LaSalle County Station, Units 1 and 2
Facility Operating License Nos. NPF-11 and NPF-18
NRC Docket Nos. 50-373 and 50-374

Subject: Justification for the Continued Use of Technical Specifications, Section 3.4.11,
"RCS Pressure and Temperature (P/T) Limits"

- Reference:
- (1) Letter from R.M. Krich (ComEd) to U. S. NRC, "Application for Amendment to Appendix A, Technical Specifications, Section 3/4.4.6, "Pressure Temperature Limits, Reactor Coolant System," and Request for Exemption from 10 CFR 50.60, "Acceptance Criteria for Fracture Prevention Measures for Lightwater Nuclear Power Reactors for Normal Operation," dated February 29, 2000
 - (2) Letter from Charles G. Pardee (ComEd) to U. S. NRC, "Supplement to Application for Amendment to Appendix A, Technical Specifications, Section 3/4.4.6, "Pressure Temperature Limits, Reactor Coolant System," and Request for Exemption from 10 CFR 50.60, "Acceptance Criteria for Fracture Prevention Measures for Lightwater Nuclear Power Reactors for Normal Operation," dated August 18, 2000
 - (3) Letter from Donna M. Skay (U. S. NRC) to O. D. Kingsley (ComEd), "LaSalle County Station, Units 1 and 2 – Issuance of Amendments (TAC Nos. MA8403 and MA8404), dated November 8, 2000.
 - (4) Letter from Charles G. Pardee (ComEd) to U. S. NRC, "Revised General Electric Nuclear Energy Reports, "Pressure Temperature Curves for ComEd LaSalle Unit 1" and "Pressure Temperature Curves for ComEd LaSalle Unit 2" dated June 26, 2000

AP01

Exelon Generation Company (EGC), LLC, formerly Commonwealth Edison (ComEd) Company, in Reference 1, requested changes to Technical Specifications (TS) Section 3/4.4.6, "Pressure/Temperature Limits, Reactor Coolant System," for LaSalle County Station Units 1 and 2. The proposed changes revised the Pressure and Temperature (P/T) limits for the Reactor Pressure Vessel (RPV) of each unit to a maximum of 32 Effective Full Power Years (EFPY).

During teleconferences between members of the NRC and EGC in support of the review of the proposed TS changes, the NRC stated that the neutron fluence calculations used to develop the revised P/T limits were not consistent with the guidance contained in Draft Regulatory Guide DG-1053, "Calculational and Dosimetry Methods for Determining Pressure Vessel Neutron Fluence," dated September 1999. EGC in Reference 2 requested the NRC to approve the proposed changes to TS 3/4.4.6 until December 15, 2002 to allow sufficient time to resolve this issue. The NRC in Reference 3 approved the proposed changes to TS 3/4.4.6 for an interim period not to exceed December 15, 2002.

In March 2001, Draft Regulatory Guide DG-1053 was approved as Regulatory Guide (RG) 1.190, "Calculational and Dosimetry Methods for Determining Pressure Vessel Neutron Fluence." In September 2001, the NRC approved the General Electric Topical Report NEDC-32983P, "General Electric Methodology for Reactor Pressure Vessel Fast Neutron Flux Evaluation," for use by licensees. The NEDC-32983P methodology is consistent with the guidance contained in RG 1.190.

EGC has performed new fluence calculations using NEDC-32983P methodology for LaSalle County Station Units 1 and 2. The results of the calculations are contained in Attachments A and B. Attachment A contains a proprietary version of the calculations and corresponding affidavit requesting withholding from public disclosure. We request the withholding of the information contained in Attachment A, in accordance with 10 CFR 2.790(a)(4). A non-proprietary version of the report is contained in Attachment B. The results of the fluence calculations are as follows.

- The 32 EFPY fluences calculated with the NEDC-32983P methodology are greater than the fluences used in the development of the current 32 EFPY P/T limits in the LaSalle County Station TS. TS 3/4.4.6 was renumbered to TS 3.4.11, "RCS Pressure and Temperature (P/T) Limits," during the conversion of LaSalle County Station TS to the Improved Technical Specification format.
- As shown in Attachment A to Reference 4, the peak surface fluence used in the development of the Unit 1 current 32 EFPY P/T limits is $5.0\text{E}17 \text{ n/cm}^2$ and the resultant $1/4 \text{ T}$ fluence is $3.5\text{E}17 \text{ n/cm}^2$. As shown in the attached report, the Unit 1 peak surface flux determined in the proposed calculation is $1.01\text{E}09 \text{ n/cm}^2\text{-s}$. A conservative estimate of the neutron surface fluence at various points in plant life can be obtained by multiplying the calculated flux by the appropriate EFPY. This approach is conservative in that it assumes that the calculated flux value has been present since initial plant operation and does not account for the reduced flux that would have been experienced prior to power uprate and the switch to 24 month fuel cycles. Using this method, the peak surface fluence of $5.0\text{E}17 \text{ n/cm}^2$ used in development of the current P/T limits will occur at approximately 15.7 EFPY.

- As shown in Attachment A to Reference 4, the peak surface fluence used in the development of the Unit 2 current 32 EFPY P/T limits is $6.03\text{E}17 \text{ n/cm}^2$ and the resultant 1/4 T fluence is $4.2\text{E}17 \text{ n/cm}^2$. As shown in the attached report, the Unit 2 peak surface flux determined in the proposed calculation is $1.08\text{E}09 \text{ n/cm}^2\text{-s}$. Using the method described above, the peak surface fluence of $6.03\text{E}17 \text{ n/cm}^2$ used in development of the current P/T limits will occur at approximately 17.7 EFPY.

Based on the above, the current P/T curves in TS 3.4.11 for LaSalle County Station Units 1 and 2 remain valid until at least 15.7 EFPY. As of June 1, 2002, LaSalle County Station Unit 1 operating time was approximately 11.6 EFPY and Unit 2 was approximately 11.0 EFPY. Considering a 100% capacity factor, 15.7 EFPY will not be reached on either unit until after June 2006.

EGC is currently scheduled to submit to the NRC a proposed change to TS 3.4.11 in the fall of 2002. The proposed changes will utilize NEDC-32983P methodology to calculate the P/T curves in TS 3.4.11 for LaSalle County Station Units 1 and 2.

Exelon requests that the current P/T curves in TS 3.4.11 remain acceptable for use until December 15, 2004, to allow sufficient time for the incorporation of the NEDC-32983P methodology into the P/T curves in TS 3.4.11 for LaSalle County Station Units 1 and 2. The request is based on the above information that using NEDC-32983P methodology, the current TS 3.4.11 P/T curves remain valid during this period of time.

If there are any questions or comments concerning this letter, please contact me at (630) 657-2821.

Sincerely,



T. W. Simpkin
Manager – Licensing
Mid-West Regional Operating Group

Attachments

- Attachment A. GE Proprietary Information, Final Report LaSalle 1 & 2 Neutron Flux Evaluation
- Attachment B. Final Report LaSalle 1 & 2 Neutron Flux Evaluation

cc: Regional Administrator – NRC Region III
NRC Senior Resident Inspector – LaSalle County Station
Office of Nuclear Facility Safety – Illinois Department of Nuclear Safety

Attachment B

Final Report
LaSalle 1 &2
Neutron Flux Evaluation



GE Nuclear Energy

GE-NE-0000-0002-5244-02

Revision 0

Class 1

June 2002

Final Report

LaSalle 1&2 Neutron Flux Evaluation

GE-NE-0000-0002-5244-02

Revision 0

Class 1

June 2002

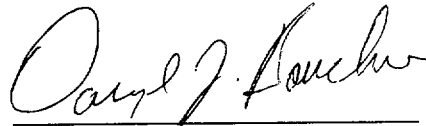
Final Report

LaSalle 1&2
Neutron Flux Evaluation

Principal Contributor:

Tang Wu

Approved by:



Daryl J. Bouchie
Technical Projects Manager

GE-NE-0000-0002-5244-02

Revision 0

Class 1

June 2002

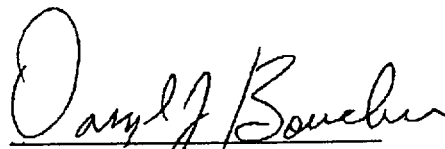
Final Report

**LaSalle 1&2
Neutron Flux Evaluation**

Principal Contributor:

Tang Wu

Approved by:

A handwritten signature in black ink, appearing to read "Darryl G. Bouchie". The signature is written over a horizontal line.

**Darryl G. Bouchie
Technical Projects Manager**

**IMPORTANT NOTICE REGARDING THE
CONTENTS OF THIS REPORT**

Please Read Carefully

A. Disclaimer

The only undertakings of the General Electric Company (GE) respecting information in this document are contained in the contract between the company receiving this document and GE. Nothing contained in this document shall be construed as changing the applicable contract. The use of this information by anyone other than a customer authorized by GE to have this document, or for any purpose other than that for which it is intended, is not authorized. With respect to any unauthorized use, GE makes no representation or warranty, and assumes no liability as to the completeness, accuracy or usefulness of the information contained in this document, or that its use may not infringe privately owned rights.

TABLE OF CONTENTS

	<u>Page</u>
ACRONYMS AND ABBREVIATIONS.....	iv
1.0 INTRODUCTION.....	1
2.0 SUMMARY AND CONCLUSIONS	2
2.1 BOUNDING FLUX FOR LASALLE 2	2
2.2 BOUNDING FLUX FOR LASALLE 1	2
2.3 ESTIMATED FLUX FOR OTHER CORES	3
2.4 NEUTRON FLUENCE	3
3.0 EVALUATION	4
3.1 SCOPE	4
3.2 INPUTS AND ASSUMPTIONS	4
3.3 METHOD OF EVALUATION.....	4
3.3.1 (R, θ) Model.....	5
3.3.2 (R,Z) Model	6
3.3.3 Material Composition and Coolant Density	7
3.3.4 Neutron Source Distribution.....	7
3.4 BIAS AND UNCERTAINTY	8
4.0 BOUNDING FLUX FOR LASALLE 2.....	14
4.1 NEUTRON FLUX AT RPV INSIDE SURFACE.....	14
4.2 NEUTRON FLUX AT SURVEILLANCE CAPSULE LOCATION	14
4.3 NEUTRON FLUX AT SHROUD INSIDE SURFACE	14
4.4 NEUTRON FLUX AT H4 WELD.....	15
5.0 BOUNDING FLUX FOR LASALLE 1.....	20
6.0 FLUX EVALUATION FOR OTHER CORES	22
6.1 CORE DATA	22
6.2 NEUTRON FLUX ESTIMATION.....	22
6.2.1 Bundle Relative Importance to Shroud and RPV Flux.....	23
6.2.2 Bundle Energy	24
6.2.3 Flux Estimation.....	25
7.0 NEUTRON FLUENCE	35
8.0 REFERENCES.....	36
APPENDIX A PLOT DATA.....	37

LIST OF TABLES

<u>Table</u>	<u>Title</u>	<u>Page</u>
Table 3-1	Design Input Data for Flux Calculation	9
Table 6-1	Comparison of Bundle Energy and Estimated Flux	26

LIST OF FIGURES

<u>Figure</u>	<u>Title</u>	<u>Page</u>
Figure 3-1.	Core Layout and Vessel Internal Components	11
Figure 3-2.	Schematic of (R,Z) Model	12
Figure 3-3.	Relative Energy by Bundle at Core Midplane – L2C9	13
Figure 4-1.	Azimuthal Distribution of Fast Neutron Flux at RPV Inside Surface – LaSalle 2 Cycle 9	16
Figure 4-2.	Axial Distribution of Fast Neutron Flux at RPV Inside Surface – LaSalle 2 Cycle 9	17
Figure 4-3.	Azimuthal Distribution of Fast Neutron Flux at Shroud Inside Surface – LaSalle 2 Cycle 9	18
Figure 4-4.	Axial Distribution of Fast Neutron Flux at Shroud Inside Surface – LaSalle 2 Cycle 9	19
Figure 5-1.	Azimuthal Distribution of Fast Neutron Flux at RPV Inside Surface – LaSalle 1 Bounding Case.....	21
Figure 6-1.	Relative Importance by Bundle for Peak Shroud Flux	27
Figure 6-2.	Relative Importance by Bundle for Peak RPV Flux	28
Figure 6-3.	Relative Cycle Energy by Bundle – L2C9.....	29
Figure 6-4.	Relative Cycle Energy by Bundle – L1C9.....	30
Figure 6-5.	Relative Cycle Energy by Bundle – L1C10.....	31
Figure 6-6.	Relative Cycle Energy by Bundle – L1C6.....	32
Figure 6-7.	Relative Cycle Energy by Bundle – L2C6.....	33
Figure 6-8.	Axial Energy Profiles of the Three Dominant Bundles	34

ACRONYMS AND ABBREVIATIONS

BAF	Bottom of Active Fuel
BOC	Beginning of Cycle
ECP	Engineering Computer Program
EFPY	Effective Full-Power Years
ENDF	Evaluated Nuclear Data File
EOC	End of Cycle
GE	General Electric
GE-NE	General Electric Nuclear Energy
IASCC	Irradiation Assisted Stress Corrosion Cracking
ID	Inside Diameter
LTR	Licensing Topical Report
MOC	Middle of Cycle
MWt	Megawatt Thermal
NRC	Nuclear Regulatory Commission
OD	Outside Diameter
ORNL	Oak Ridge National Laboratory
RPV	Reactor Pressure Vessel

1.0 INTRODUCTION

Neutron irradiation of the reactor pressure vessel (RPV) causes reduction in material ductility and creates structural embrittlement at higher operating temperatures. The effect is particularly significant when impurities such as nickel, copper, or phosphorus are present in noticeable levels, as commonly true for the RPV steel. Therefore determination of neutron fluence level is one of the first steps toward RPV fracture toughness evaluations.

Irradiation by fast neutrons (with energies greater than 1 MeV) can also be a concern with respect to irradiation assisted stress corrosion cracking (IASCC) for reactor internal components such as core shroud, top guide, core plate, etc. Crack growth evaluation for these components also requires adequate determination of neutron fluence level.

Neutron flux, or fluence rate, can be determined through radiochemical analysis of the surveillance flux wire samples; which are made of iron, copper, or nickel, sealed inside a capsule and held in place by a holder near the RPV inside surface. The calculated ratio of surveillance sample flux to the RPV peak flux defines a lead factor. This lead factor can be applied to the sample dosimetry data to determine the RPV peak flux.

Neutron flux can also be determined by solving the neutron transport equation with the discrete ordinates method or Monte Carlo simulation. When appropriate bias is applied to the calculation results, these numerical methods can be used to obtain the best-estimate flux distribution.

The objective of this work is to evaluate the neutron flux distributions at the RPV and at the shroud that bound the LaSalle Unit 1 and Unit 2 plants at the currently licensed power of 3489 MWt. The other objective is to provide flux estimates for a representative future cycle and pre-uprated cycles to determine whether these cycles are bounded by the fluxes from the bounding calculation. Once the neutron flux is determined, the lifetime fluence can be assessed by summing up the cycle-dependent neutron fluence, which is the product of cycle-specific neutron flux level and the effective-full-power days of each cycle.

2.0 SUMMARY AND CONCLUSIONS

2.1 Bounding Flux for LaSalle 2

The methodology used for the neutron flux calculation is documented in the GE's Licensing Topical Report (LTR) NEDO-32983-A [1], which was approved by the U.S. NRC for licensing applications in the Safety Evaluation Report [2]. In general, GE's methodology described in the LTR adheres to the guidance in Regulatory Guide 1.190 [3] for neutron flux evaluation. In this evaluation, the fast neutron flux distribution is calculated based on the three-dimensional flux synthesis of two separate two-dimensional flux solution calculations performed in an (r,z) and an (r, θ) model. These flux solution calculations are performed using the two-dimensional discrete ordinates code DORT [4]. The operating condition assumed for the bounding analysis is based on the LaSalle 2 Cycle 9 core data [5]. The analysis inputs have been concurred by Exelon in the transmittal of design input request [6]. The core power used is the currently licensed power of 3489 MWt.

The calculated peak fast flux ($E > 1$ MeV) at the RPV inside surface is $1.08\text{E}9$ n/cm²-s (neutrons per square centimeter per second). The peak flux is located at the elevation of 93 inches above the BAF and at azimuths of 26° and 64° past the quadrant reference of 0°, 90°, 180°, and 270° vessel azimuths.

The calculated fast flux at the capsule center is $1.07\text{E}9$ n/cm²-s for the 30° capsule. Flux for the 120° and 300° capsules is not expected to be different from the 30° capsule because of symmetry in core power and geometry, and similarity of shadowing by jet pump risers at these locations. The calculated lead factor for the RPV inside surface is 0.99.

The peak fast flux for the shroud inside surface (nominal ID) is $2.90\text{E}12$ n/cm²-s. The peak flux is located at the elevation of 97.3 inches above the BAF and at angles of 24.5° and 65.5° past the quadrant reference.

The peak fast flux for the shroud inside surface (nominal ID) at the H4 weld elevation is $2.79\text{E}12$ n/cm²-s.

2.2 Bounding Flux for LaSalle 1

The bounding flux evaluation for LaSalle 1 is based on the L2C9 core data, but with the Unit 1 vessel dimension. The Unit 1 vessel is slightly larger than Unit 2 (254 inches in base metal inside diameter, compared to 253.375 inches for Unit 2).

The calculated peak fast flux for the RPV inside surface is $1.01\text{E}9$ n/cm²-s, a reduction of approximately 7% from the LaSalle Unit 2 analysis. The peak flux is located at

azimuths of 26° and 64° past the quadrant reference. The calculated fast flux at the capsule center is 1.02E9 n/cm²-s for the 30° capsule. The calculated lead factor is 1.01.

The shroud flux is unaffected by the vessel dimension and, therefore, Unit 1 and Unit 2 have the same bounding shroud and H4 weld fluxes.

2.3 Estimated Flux for Other Cores

Several LaSalle cores have been evaluated; including a post-uprate cycle for Unit 1 (L1C9), a proposed future cycle (L1C10), and two pre-uprated cores when the surveillance capsules were last removed (L1C6 and L2C6).

The results of this evaluation show that the RPV flux for L1C9 and L1C10 is about 85% of the L2C9. L1C6 and L2C6 show considerably lower estimated RPV fluxes (53% and 65% of L2C9, respectively), as these cores have significantly lower power in the peripheral bundles. The shroud fluxes show a similar trend.

2.4 Neutron Fluence

Bounding fluxes are used to provide a conservative estimate of the neutron fluences at the end of plant life of 32 Effective Full-Power Years (EFPY). The peak 32-EFPY fluence at the RPV inside surface is 1.02E18 n/cm² for LaSalle 1 and 1.09E18 n/cm² for LaSalle 2. The peak 32-EFPY fluence at the shroud inside surface is 2.93E21 n/cm² for both LaSalle 1 and 2.

3.0 EVALUATION

3.1 Scope

Fast neutron fluxes in the beltline region extending from the core through the RPV are calculated in this analysis. This bounding calculation is based on the LaSalle 2 Cycle 9 (L2C9) core data. In addition, a bounding flux calculation is performed for LaSalle 1, based on the L2C9 core data and the Unit 1 vessel dimension.

Additional evaluation is performed to provide flux estimates for a representative future cycle and pre-uprated cycles to determine whether these cycles are bounded by the fluxes from the bounding calculation. Once the neutron flux is determined, the lifetime fluence can be determined by summing up the cycle-dependent neutron fluences, which are the product of cycle-specific neutron flux level and the effective-full-power days of each cycle.

3.2 Inputs and Assumptions

The operating condition assumed for the LaSalle 2 bounding analysis is based on the LaSalle 2 Cycle 9 core data [5]. It is noted that these data are projected values [5] and not the actual cycle data. These core design data are contained in the hard-copy material of core loading and bundle names, as well as electronic copies of bundle types, bundle heavy metal mass, and void and exposure data at the BOC and EOC. Pertinent data from these files are processed as part of the input data preparation for the flux calculation. The core power used is the currently licensed power of 3489 MWt.

The RPV and shroud dimensions, together with the configuration and location of surveillance capsule holder, are provided in Reference 6 and shown in Table 3-1.

3.3 Method of Evaluation

The methodology used for the neutron flux calculation is documented in a Licensing Topical Report (LTR) NEDO-32983-A [1], which was approved by the U.S. NRC in the Safety Evaluation Report for referencing in licensing actions [2]. In general, GE's methodology described in the LTR adheres to the guidance in Regulatory Guide 1.190 [3] for neutron flux evaluation.

The flux calculations are performed with DORTG01V, which is a discrete ordinates code package based on CCC-543 TORT-DORT Version 2.8.14 issued by Oak Ridge National Laboratory (ORNL) in 1984 [4]. DORTG01V is a controlled version of DORT in the GE Engineering Computation Program (ECP) library. The NRC has approved the use of DORT as part of the GE methodology.

The cross-section data used in the DORTG01V calculation are processed with the nuclear cross-section processing package in the GE ECP.

Mixture macroscopic cross sections were then created by combining the microscopic cross sections with nuclide densities. This data set is further transformed to a group-organized mixture cross-section format compatible with the DORT inputs. A P_3 truncation of the Legendre polynomial expansion, which is a common practice for the BWR RPV flux calculation, is used to approximate the anisotropy in the differential scattering cross sections. The approach discussed here is consistent with the approved LTR methodology.

3.3.1 (R, θ) Model

LaSalle 2 Cycle 9 core is the basis of the bounding flux evaluation. The core load contains 160 bundles of GE9, 256 bundles of Atrium-9 with 80-mil channels, and 348 bundles of Atrium-9 with 100-mil channels. Fuel bundles in the outermost row contain only 8x8 GE9 fuels. A quadrant of the core and the vessel internal components that are relevant to the flux calculation is illustrated in Figure 3-1.

In the angular coordinate θ , the mesh size is $\frac{1}{2}$ degree per mesh interval, except for the two boundary nodes, which is $\frac{1}{4}$ degree. For a core quadrant, a total of 181 fine meshes are used in the θ -direction.

Radial meshes vary in sizes. Generally, a fine mesh is provided near material interfaces, where significant flux gradients are expected. Fine meshes are also applied near the shroud and the capsule. Sufficient fine mesh steps are provided to simulate the outer boundary profiles of the core. The mesh step is fine enough such that the actual core boundary can be approximated to the nearest 0.8 cm.

The (r,θ) calculation is performed for the first quadrant of the reactor. The model includes three sets of jet-pump/riser, which are centered at 30° , 60° , and 90° . It also includes the 30° capsule, which is completely shadowed by the jet-pump riser. The azimuthal distribution of RPV flux in the first quadrant is expected to be representative of other quadrants because of the quadrant symmetry in the power distribution. However, the RPV flux at 0 and 180 degrees is expected to be higher than the flux at 90 and 270 degrees, due to the difference in the jet-pump shadowing effect.

3.3.2 (R,Z) Model

3.3.3 Material Composition and Coolant Density

Material compositions in each calculation model are treated as homogeneous mixtures. The volume fractions of solid material in the three core regions are calculated based on specific fuel bundle design data.

3.3.4 Neutron Source Distribution

The energy produced per fission and the neutron yield data that correspond to the middle-of-cycle (MOC) exposure were obtained from TGBLA calculations. These data are

then used to generate the total neutron source in the core. Spatial distribution of the neutron source density is simulated based on relative cycle-integrated energy production.

Figure 3-3 shows the bundle-dependent relative cycle energy (normalized to the core average) at core midplane elevation (axial node 13). These discrete data in the (x,y) plane are processed to form the neutron source distribution in the (r, θ) meshes for the (r, θ) calculation. Due to the utilization of a 24-month fuel cycle, the power densities of the peripheral bundles are relatively high. This will have significant impact on the shroud and RPV flux levels. For the (r,z) calculation, the axial and radial distribution of relative nodal energy along the 25° azimuth is used.

3.4 Bias and Uncertainty

Table 3-1 Design Input Data for Flux Calculation

Parameter	Unit 1 Data	Unit 2 Data	Reference Drawing
(A) Surveillance Capsules			
Azimuths, degrees	30, 120, 300	Same as Unit 1	105D4719
Width	7.06"	Same as Unit 1	117C4335 P002
Basket Thickness	0.99"	Same as Unit 1	"
Basket Center to Clad	0.875"	Same as Unit 1	919D988AC Sh 4, 129B3157 P001
Basket Height	13.315"	Same as Unit 1	117C4335 P002, 129B3157 P001
Basket Center Elevation (above Bottom of Active Fuel (BAF))	73.558"	Same as Unit 1	117C4335 P002, 919D988AC Sh 4, 129B3157 P001
(B) RPV (Beltline)			
RPV Minimum ID (Base Metal)	254"	253.375"	L1: CE# 232-788 R3 (GE VPF# 2029-117 R4) L2: CBI# 1, R7 (GE VPF# 3073-1 R7)
RPV Thickness (min.)	6.125"	6.1875"	"
Clad Thickness (nom.)	0.3125"	0.1875"	"
(C) Shroud (Active Fuel Region)			
Shroud ID	203.12"±0.50"	Same as Unit 1	761E763
Shroud Thickness	2"	Same as Unit 1	"
Elevation of H4 Weld	297.0"	Same as Unit 1	L1: VPF 2029-082 R5 and 105E11347B R0 L2: 732E143 R16 and 107E5313G R0]

Table 3-1 Design Input Data for Flux Calculation (Cont.)

Parameter	Unit 1 Data	Unit 2 Data	Reference Drawing
(D) Jet Pump Components			
Recirc. Inlet Nozzles Azimuths, degrees	30, 60, 90, 120, 150, 210, 240, 270, 300, 330	Same as Unit 1	L1: 919D988AC Sh 1 R17. L2: 732E143 Sh 1 R16
Jet Pump Riser Pipe	10" Schd. 30	Same as Unit 1	117C2809 P1
Jet Pump Inlet Mixer OD	7.17"	Same as Unit 1	762E189 R3
Jet Pump Inlet Mixer ID	6.40"	Same as Unit 1	105E4755 G002
Radial Location of Jet Pump Riser from Core Center	112.28"	Same as Unit 1	105E1881 Sh 1 R0
Distance between Riser and Inlet Mixer, centerline to centerline	14.75"	Same as Unit 1	762E189 R3
(E) Reactor Core			
BWR Type	BWR/5	Same as Unit 1	
Fuel Bundles	764	Same as Unit 1	
Bundle Pitch	6"	Same as Unit 1	
Active Fuel Length	150" (GE9), 149" (Atrium)	Same as Unit 1	
Elevation of BAF	216.313"	Same as Unit 1	
Density of Downcomer Water	0.7572 g/cm ³	Same as Unit 1	
Density of Bypass Water between Shroud and Fuel Bundles	0.7375 g/cm ³	Same as Unit 1	

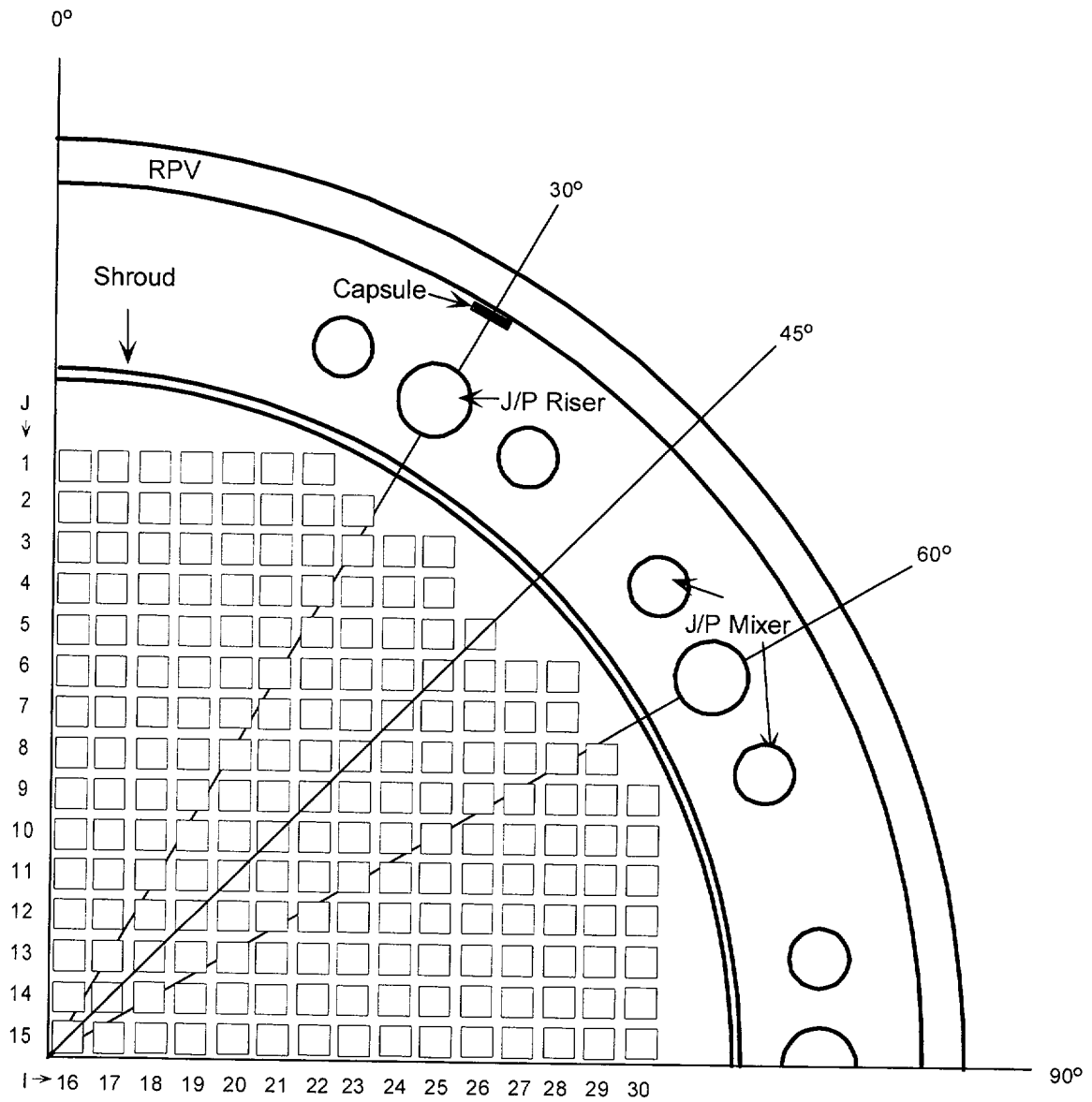
Figure 3-1. Core Layout and Vessel Internal Components

Figure 3-2. Schematic of (R,Z) Model

Figure 3-3. Relative Energy by Bundle at Core Midplane – L2C9

J=	I=	16	17	18	19	20	21	22	23	24	25	26	27	28	29	30
1		0.6621	0.6871	0.6828	0.6752	0.6132	0.5568	0.4831								
2		1.2873	1.3051	1.2143	1.2825	1.2329	1.1524	0.9048	0.5964							
3		1.2107	1.3992	1.3713	1.3888	1.2378	1.2874	1.2614	0.9995	0.5918	0.4279					
4		1.0480	1.3974	1.4590	1.3937	1.1016	1.2897	1.3042	1.2317	1.1140	0.6090					
5		1.4526	1.4973	1.4206	1.4797	1.4081	1.3450	1.3291	1.3585	1.2192	0.9626	0.5713				
6		1.3995	1.3907	1.5167	1.5044	1.1112	1.4884	1.4923	1.4317	1.2302	0.9725	0.9635	0.6109	0.4270		
7		1.0431	1.4312	1.5045	1.2569	1.0440	1.4623	1.5189	1.3850	1.0811	1.2297	1.2209	1.1142	0.5918		
8		1.2815	1.5451	1.5152	1.3417	1.2538	1.4869	1.4132	1.3532	1.3857	1.4331	1.3603	1.2338	0.9993	0.5949	
9		1.4852	1.4080	1.4942	1.5050	1.4920	1.4768	1.4026	1.4134	1.5181	1.4932	1.3293	1.3061	1.2628	0.9049	0.4832
10		1.3667	1.4596	1.3915	1.5189	1.3885	1.3968	1.4767	1.4875	1.4622	1.4897	1.3466	1.2908	1.2889	1.1535	0.5551
11		1.0127	1.3631	1.4548	1.1805	0.9983	1.3880	1.4924	1.2557	1.0479	1.1105	1.4079	1.1026	1.2409	1.2339	0.6130
12		1.2323	1.4596	1.3785	0.9843	1.1809	1.5192	1.5036	1.3414	1.2570	1.5049	1.4795	1.3932	1.3903	1.2831	0.6774
13		1.4682	1.4596	1.3827	1.3766	1.4553	1.3909	1.4936	1.5139	1.5032	1.5170	1.4218	1.4588	1.3704	1.2139	0.6825
14		1.3829	1.4556	1.4604	1.4602	1.3666	1.4610	1.4075	1.5446	1.4310	1.3916	1.4967	1.3973	1.3977	1.3030	0.6879
15		1.0088	1.3819	1.4683	1.2315	1.0128	1.3689	1.4846	1.2790	1.0468	1.4007	1.4508	1.0467	1.2096	1.2825	0.6568

4.0 BOUNDING FLUX FOR LASALLE 2

4.1 Neutron Flux at RPV Inside Surface

The calculated peak fast flux ($E > 1$ MeV) at the RPV inside surface is $1.08\text{E}9$ n/cm²-s. The azimuthal flux profile for the RPV is illustrated in Figure 4-1. The peak flux is located at azimuths of 26° and 64° past the quadrant reference of 0°, 90°, 180°, and 270° vessel azimuths. The effects of inelastic scattering by steel in the jet-pump components are clearly displayed in Figure 4-1, where the flux depression occurs in regions shadowed by metal components. The flux level at 90° is slightly lower than its mirror image at 0° due to the shadowing effect of the jet-pump riser at 90°.

Axial flux variation at the RPV inside surface is shown in Figure 4-2. The elevation of peak flux occurs at 93 inches above the BAF. The ratio of peak flux to midplane (75 inches above BAF) flux is 1.044.

4.2 Neutron Flux at Surveillance Capsule Location

The calculated fast flux ($E > 1$ MeV) at the capsule center is $1.07\text{E}9$ n/cm²-s for the 30° capsule. Flux for the 120° and 300° capsules is not expected to be different from the 30° capsule because of symmetry in core power and geometry, and similarity of shadowing by jet pump risers at these locations. The calculated lead factor for the RPV inside surface is

$$1.07\text{E}9 / 1.08\text{E}9 = 0.99.$$

This lead factor is a product of three spatial factors – radial, azimuthal, and axial, reflecting the positional differences between the surveillance capsule and the peak RPV flux. The axial factor is 0.95, which is due to the difference in the elevation between the capsule and the peak flux. The azimuthal factor is 0.80, based on the ratio of 30° flux and 26° flux at the RPV inside surface. The radial factor is approximately 1.31, due to the fact that the capsule center is 1.06 inches radially closer to the core than the RPV base metal.

4.3 Neutron Flux at Shroud Inside Surface

The calculated peak fast flux ($E > 1$ MeV) at the shroud inside surface (nominal ID of 203.12 inches) is $2.90\text{E}12$ n/cm²-s. The azimuthal flux profile for the first quadrant of the shroud is illustrated in Figure 4-3. The peak flux is located at angles of 24.5° and 65.5° in the first quadrant due to the close proximity of peripheral bundle at these angles. Flux distributions for the other three quadrants are the same as the first quadrant as a result of quadrant symmetry of the core design.

Axial flux variation at the shroud inside surface is shown in Figure 4-4. The elevation of peak flux occurs at 97.3 inches above the BAF. The ratio of peak flux to midplane flux is 1.071.

4.4 Neutron Flux at H4 Weld

The peak fast flux for the shroud inside surface (nominal ID) at the H4 weld elevation is

$$(2.90\text{E}12 \text{ n/cm}^2\text{-s}) (0.963) = 2.79\text{E}12 \text{ n/cm}^2\text{-s}.$$

Figure 4-1. Azimuthal Distribution of Fast Neutron Flux at RPV Inside Surface – LaSalle 2 Cycle 9

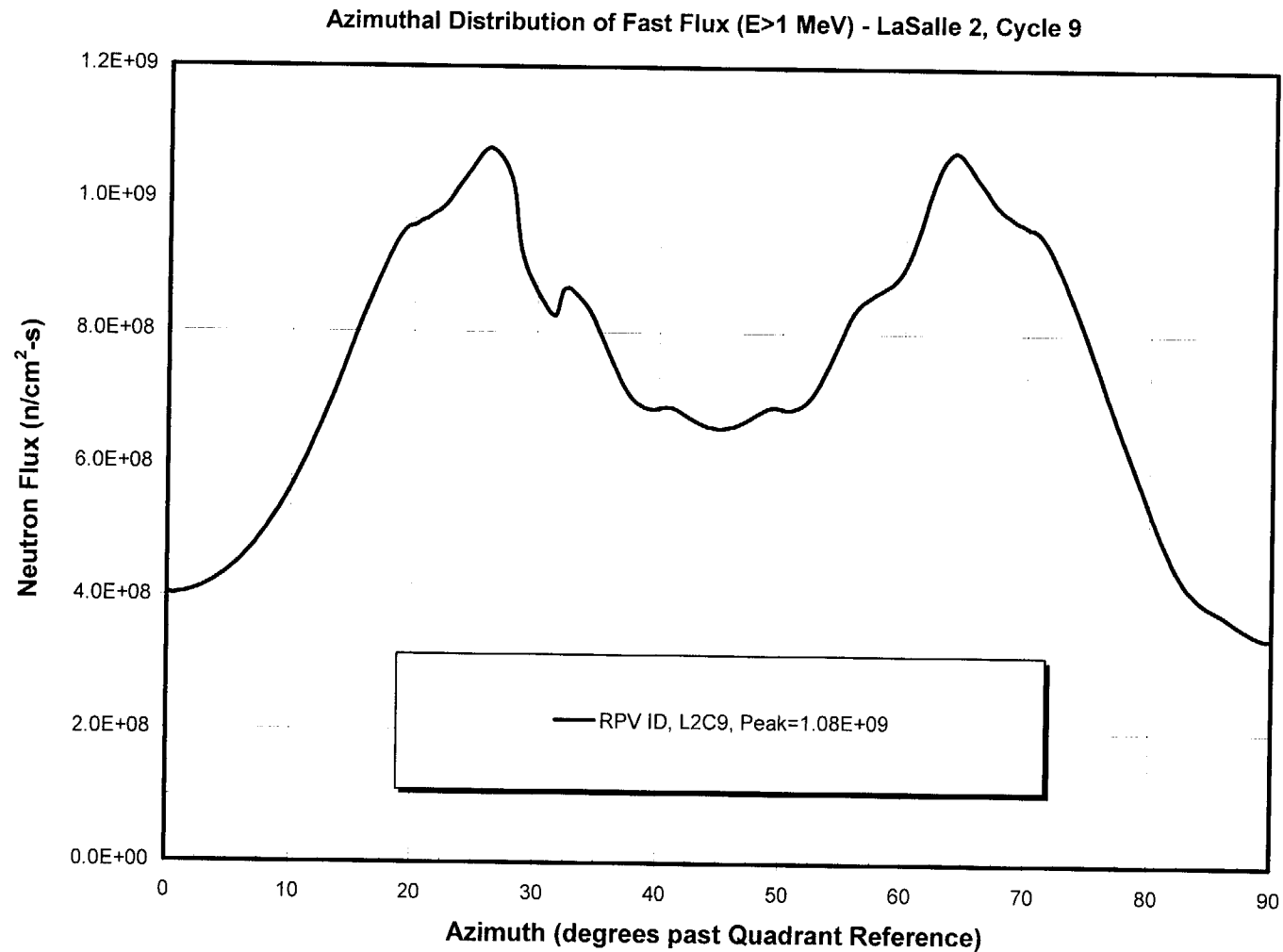


Figure 4-2. Axial Distribution of Fast Neutron Flux at RPV Inside Surface – LaSalle 2 Cycle 9

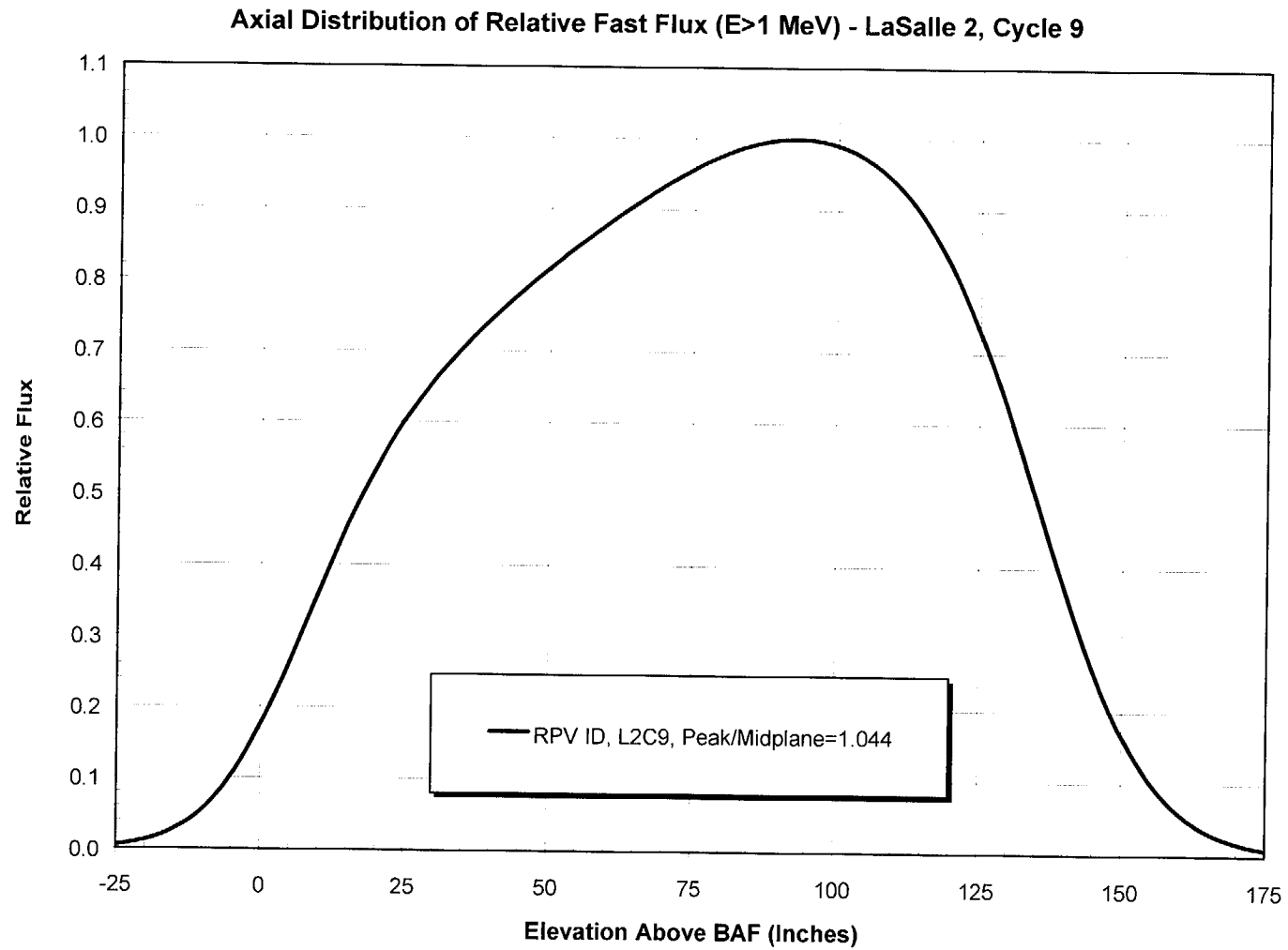


Figure 4-3. Azimuthal Distribution of Fast Neutron Flux at Shroud Inside Surface – LaSalle 2 Cycle 9

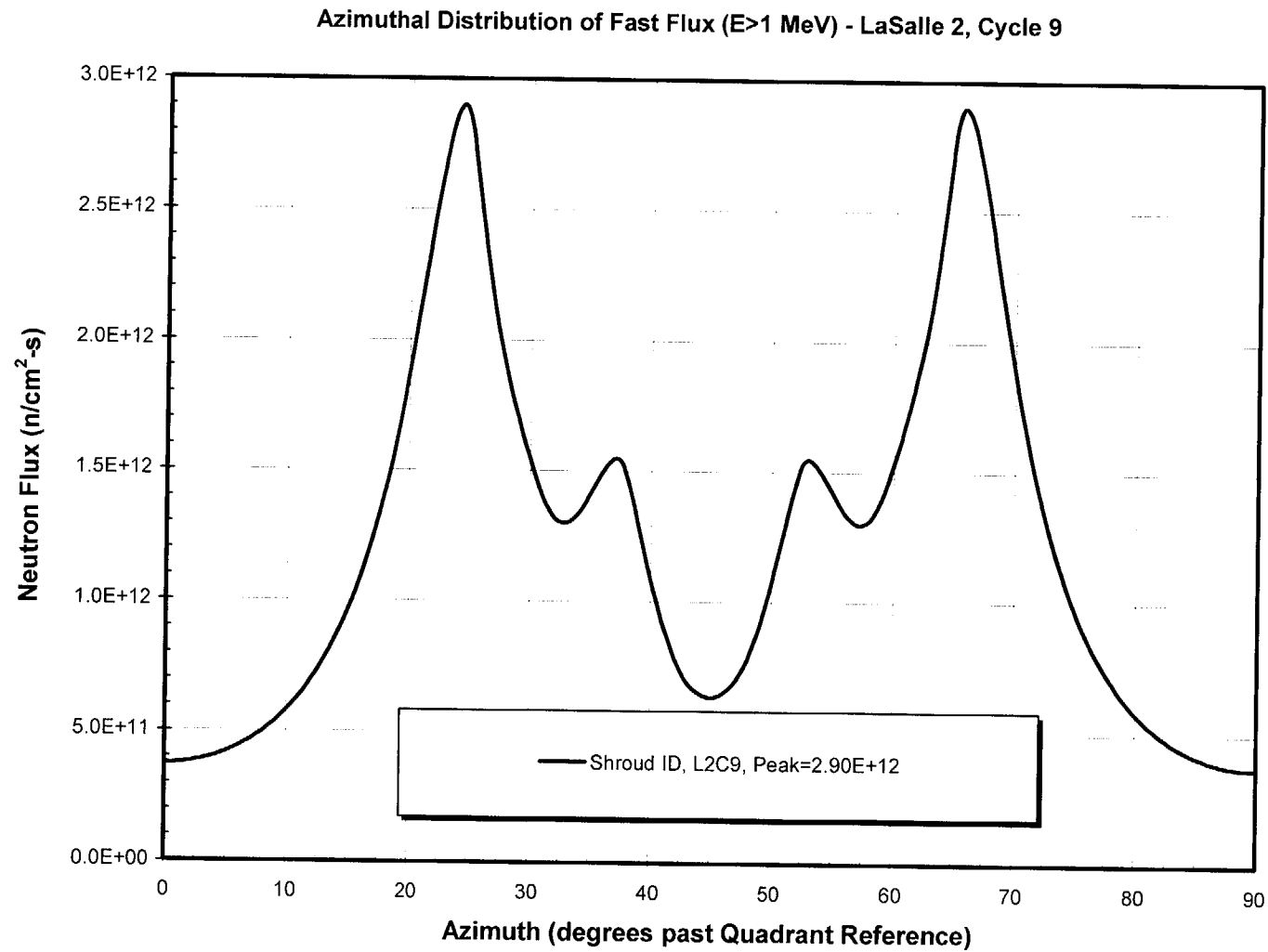
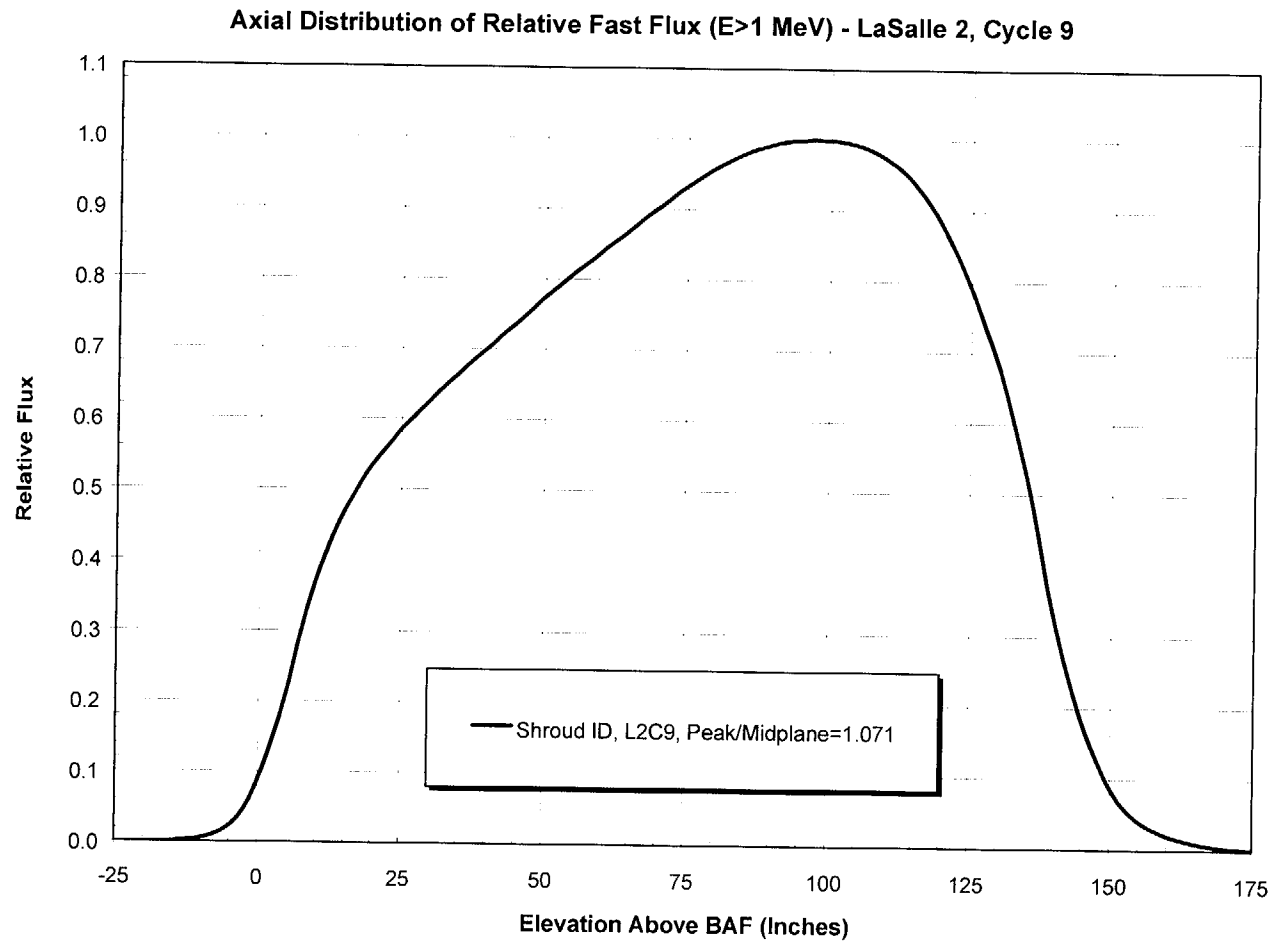


Figure 4-4. Axial Distribution of Fast Neutron Flux at Shroud Inside Surface – LaSalle 2 Cycle 9



5.0 BOUNDING FLUX FOR LASALLE 1

The bounding flux evaluation for LaSalle 1 is based on the L2C9 core data, but with the Unit 1 vessel dimension. From Table 3-1 data, the differences in the vessel dimension between Unit 1 and Unit 2 are the following:

	Unit 2	Unit 1	Difference
RPV Minimum ID (Base Metal)	253.375"	254"	0.625"
Clad Thickness (nom.)	0.188"	0.313"	0.125"
RPV Thickness (min.)	6.188"	6.125"	-0.063"

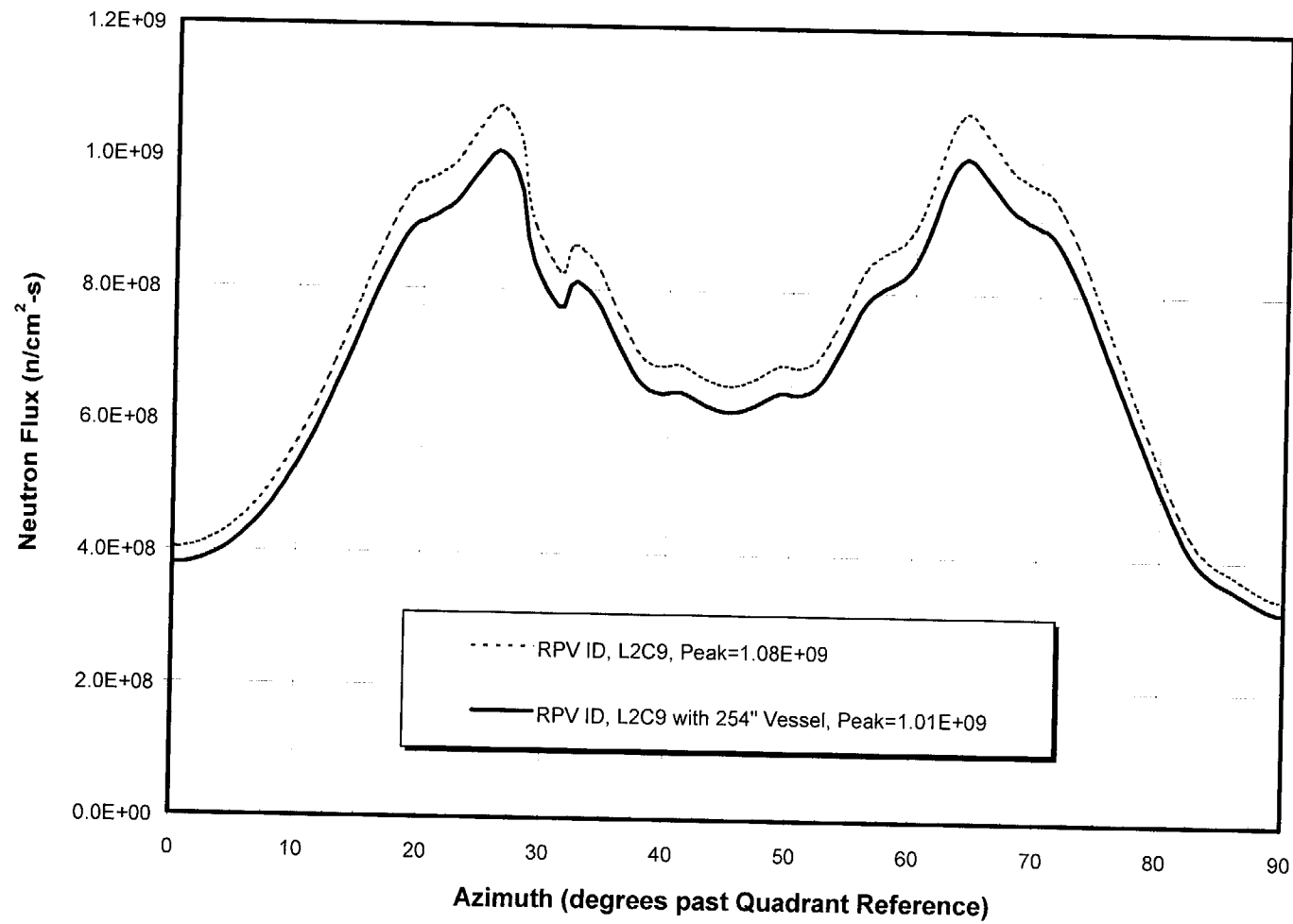
Since the radial position of the capsule holder is determined from the radial gap between the holder and the vessel cladding, the radial position for the capsule center for Unit 1 is expected to be larger than that of the Unit 2 by 0.188" ($0.625"/2 - 0.125"$), while the radial difference for the base metal is 0.313". On the other hand, the locations of jet-pump components are specified in reference to core center and are independent of vessel dimension. Therefore, Unit 1 and Unit 2 have identical jet-pump dimensions.

Results from the (r,z) calculation indicate that the axial flux distribution at the RPV inside surface does not change with the slight increase of vessel dimension.

Figure 5-1 shows the azimuthal variation of fast neutron flux ($E > 1$ MeV) at the RPV inside surface. The results for the L2C9 calculation are also shown for comparison. The peak fast flux for the RPV inside surface is $1.01E9$ n/cm²-s at angles of 26° and 64°. That is, the peak flux is reduced by approximately 7% from the Unit 2 analysis of $1.08E9$ n/cm²-s. The capsule flux is $1.02E9$ n/cm²-s, a reduction of approximately 5% from the Unit 2 analysis of $1.07E9$ n/cm²-s. Consequently, the lead factor is 1.01, a slight increase from the Unit 2 analysis of 0.99. The three contributing factors for the lead factor are 0.95 axial, 0.79 azimuthal, and 1.34 radial.

The shroud flux is unaffected by the vessel dimension and, therefore, Unit 1 and Unit 2 have the same bounding shroud and H4 weld fluxes.

Figure 5-1. Azimuthal Distribution of Fast Neutron Flux at RPV Inside Surface – LaSalle 1 Bounding Case



6.0 FLUX EVALUATION FOR OTHER CORES

An evaluation has been performed to assess the relative flux values for the following LaSalle cores:

- Post-uprated core: LaSalle 1 Cycle 9 (L1C9).
- Proposed future core: LaSalle 1 Cycle 10 (L1C10).
- Representative pre-updated core when the last removed surveillance capsule was present: LaSalle 1 Cycle 6 (L1C6) and LaSalle 2 Cycle 6 (L2C6).

This evaluation is based on comparing the critical characteristics of each core that have significant impacts on the RPV flux and shroud flux. Generally speaking, the RPV and shroud flux are influenced by the plant design data such as vessel and shroud dimensions, location and size of jet-pump components, power level, core nodal power distribution, water density distribution in the core and the downcomer.

6.1 Core Data

Core data for the LaSalle plants are contained in the files sent by Exelon [5, 8, 9]. These data included the hard-copy material of core loading and bundle names, as well as electronic copies of bundle types, bundle heavy metal mass, and void and exposure data at the BOC and EOC.

L1C9 is similar to L2C9. The core load contains GE9 fuel with either 80-mil or 100-mil channels and Atrium-9 fuel with either 80-mil or 100-mil channels. The core data provided are projected values, not the actual cycle data.

L1C10 is the proposed future core containing 10x10 Atrium-10 fuel. The core load contains 46 bundles of GE9 with 80-mil channels, 36 bundles of Atrium-9 with 80-mil channels, 336 bundles of Atrium-9 with 100-mil channels, and 346 bundles of Atrium-10 with 100-mil channels. The outermost row of the core only contains GE9 fuel.

L1C6 contains 8x8 GE7, GE8, and GE9 fuel bundles. Similarly, L2C6 contains only GE8 and GE9 fuel bundles. These early GE designs do not use part-length rods so the axial variation of heavy metal mass is small.

6.2 Neutron Flux Estimation

6.2.1 Bundle Relative Importance to Shroud and RPV Flux

6.2.2 Bundle Energy

Similar to the flux calculation for L2C9 documented in Section 3.3.4, Equation 3-1 is used to process the heavy metal mass data and the BOC and EOC exposure data to form the relative cycle energy distribution for each core analyzed. Figures 6-3 through 6-7 show the relative cycle energy by bundle (normalized to the core average) for L2C9, L1C9, L1C10, L1C6, and L2C6.

Figure 6-8 shows a comparison of the axial nodal distribution of cycle energy for the average of the three dominant bundles at (I=22, J=1), (I=21, J=1), and (I=23, J=2), which have the most contribution to the RPV flux. Examination of these plots lead to the following preliminary indications:

- The power in the dominant peripheral bundles for the pre-uprated cycles (L1C6 and L2C6) is significantly lower than the current cycle. This difference can be attributed to the difference in the fuel management scheme. Both L1C6 and L2C6 have an 18-month refueling cycle. The small batch fraction made possible to place “dead” bundles in the core periphery. The post-uprated fuel management in LaSalle employs a 24-month cycle, leading to the placement of relatively reactive bundles in the outermost row of the core. This fuel management difference is the principal reason that the fast neutron flux for the pre-updated cores will be significantly lower than the post-uprated core.
- The proposed future cycle (L1C10) has significant number of Atrium-10 bundles in the core load. With the part-length rods in Atrium-10, the cycle energy distribution is peaked near the core midplane, instead of above the core midplane elevation typically for cores without part-length fuel rods. The axial distribution of the RPV flux should also follow this trend.

6.2.3 Flux Estimation

Estimations for the peak shroud flux and the peak RPV flux are performed by combining data in Figures 6-1 and 6-2 and the bundle energy data in Figures 6-3 through 6-7. The calculated results are shown in Table 6-1.

Table 6-1 results show that the estimated shroud and RPV fluxes from L2C9 bound other cores. The RPV flux for L1C9 and L1C10 is about 85% of the L2C9. L1C6 and L2C6 show considerably lower estimated RPV fluxes (53% and 65% of L2C9, respectively), as these cores have significantly lower power in the peripheral bundles. The shroud fluxes show similar trend.

Table 6-1 Comparison of Bundle Energy and Estimated Flux

	L2C9	L1C9	L1C10	L1C6	L2C6
Calculated Data					
Relative Bundle Energy					
Dominant Bundle (I=22, J=1)	0.373	0.317	0.309	0.203	0.227
Three Bundle Average*	0.424	0.373	0.389	0.241	0.273
Estimated Flux (Arbitrary Unit)					
Shroud ID	0.783	0.687	0.684	0.447	0.507
RPV ID	1.795	1.631	1.604	1.082	1.226
Ratio to L2C9					
Relative Bundle Energy					
Dominant Bundle (I=22, J=1)	1.00	0.85	0.83	0.54	0.61
Three Bundle Average*	1.00	0.88	0.92	0.57	0.64
Estimated Flux**					
Shroud ID	1.00	0.88	0.87	0.57	0.65
RPV ID	1.00	0.91	0.89	0.60	0.68
Estimated Flux (Net)***					
Shroud ID	1.00	0.88	0.87	0.54	0.62
RPV ID	1.00	0.85	0.83	0.53	0.65

* Bundles (I=22, J=1), (I=21, J=1), (I=23, J=2)

** With Unit 2 dimension & post-uprate power

*** Including the effect of power uprate (0.95 for pre-uprated cycles) and vessel dimension effect (0.93 for Unit 1).

Figure 6-1. Relative Importance by Bundle for Peak Shroud Flux

0.600 = Fractional Contribution for Peak bundle

J=	I= 16	17	18	19	20	21	22	23	24	25	26	27	28	29	30
1	0.000	0.000	0.002	0.007	0.035	0.190	1.000								
2	0.000	0.000	0.001	0.004	0.015	0.053	0.126	0.129							
3	0.000	0.000	0.001	0.002	0.005	0.012	0.022	0.022	0.013	0.005					
4	0.000	0.000	0.000	0.001	0.001	0.003	0.004	0.004	0.003	0.002					
5	0.000	0.000	0.000	0.000	0.000	0.001	0.001	0.001	0.001	0.000	0.000				
6	0.000	0.000	0.000	0.000	0.000	0.000	0.000	0.000	0.000	0.000	0.000	0.000	0.000		
7	0.000	0.000	0.000	0.000	0.000	0.000	0.000	0.000	0.000	0.000	0.000	0.000	0.000	0.000	
8	0.000	0.000	0.000	0.000	0.000	0.000	0.000	0.000	0.000	0.000	0.000	0.000	0.000	0.000	0.000
9	0.000	0.000	0.000	0.000	0.000	0.000	0.000	0.000	0.000	0.000	0.000	0.000	0.000	0.000	0.000
10	0.000	0.000	0.000	0.000	0.000	0.000	0.000	0.000	0.000	0.000	0.000	0.000	0.000	0.000	0.000
11	0.000	0.000	0.000	0.000	0.000	0.000	0.000	0.000	0.000	0.000	0.000	0.000	0.000	0.000	0.000
12	0.000	0.000	0.000	0.000	0.000	0.000	0.000	0.000	0.000	0.000	0.000	0.000	0.000	0.000	0.000
13	0.000	0.000	0.000	0.000	0.000	0.000	0.000	0.000	0.000	0.000	0.000	0.000	0.000	0.000	0.000
14	0.000	0.000	0.000	0.000	0.000	0.000	0.000	0.000	0.000	0.000	0.000	0.000	0.000	0.000	0.000
15	0.000	0.000	0.000	0.000	0.000	0.000	0.000	0.000	0.000	0.000	0.000	0.000	0.000	0.000	0.000

Figure 6-2. Relative Importance by Bundle for Peak RPV Flux

0.3017 = Fractional Contribution for Peak bundle

J=	I=	16	17	18	19	20	21	22	23	24	25	26	27	28	29	30
1		0.001	0.005	0.016	0.050	0.150	0.414	1.000								
2		0.001	0.002	0.007	0.020	0.053	0.128	0.270	0.475							
3		0.000	0.001	0.003	0.007	0.017	0.038	0.072	0.115	0.152	0.161					
4		0.000	0.000	0.001	0.002	0.005	0.011	0.019	0.029	0.036	0.038					
5		0.000	0.000	0.000	0.001	0.002	0.003	0.005	0.007	0.009	0.009	0.008				
6		0.000	0.000	0.000	0.000	0.001	0.001	0.001	0.002	0.002	0.002	0.002	0.002	0.001		
7		0.000	0.000	0.000	0.000	0.000	0.000	0.000	0.001	0.001	0.001	0.001	0.000	0.000		
8		0.000	0.000	0.000	0.000	0.000	0.000	0.000	0.000	0.000	0.000	0.000	0.000	0.000	0.000	
9		0.000	0.000	0.000	0.000	0.000	0.000	0.000	0.000	0.000	0.000	0.000	0.000	0.000	0.000	0.000
10		0.000	0.000	0.000	0.000	0.000	0.000	0.000	0.000	0.000	0.000	0.000	0.000	0.000	0.000	0.000
11		0.000	0.000	0.000	0.000	0.000	0.000	0.000	0.000	0.000	0.000	0.000	0.000	0.000	0.000	0.000
12		0.000	0.000	0.000	0.000	0.000	0.000	0.000	0.000	0.000	0.000	0.000	0.000	0.000	0.000	0.000
13		0.000	0.000	0.000	0.000	0.000	0.000	0.000	0.000	0.000	0.000	0.000	0.000	0.000	0.000	0.000
14		0.000	0.000	0.000	0.000	0.000	0.000	0.000	0.000	0.000	0.000	0.000	0.000	0.000	0.000	0.000
15		0.000	0.000	0.000	0.000	0.000	0.000	0.000	0.000	0.000	0.000	0.000	0.000	0.000	0.000	0.000

Figure 6-3. Relative Cycle Energy by Bundle – L2C9

J=	I=	16	17	18	19	20	21	22	23	24	25	26	27	28	29	30
1		0.5201	0.5442	0.5408	0.5381	0.4780	0.4315	0.3726								
2		1.0137	1.0307	0.9792	1.0147	0.9706	0.8993	0.7086	0.4689							
3		0.9874	1.1196	1.1046	1.1137	1.0041	1.0307	0.9992	0.7915	0.4562	0.3226					
4		0.8508	1.1294	1.1647	1.1264	0.8801	1.0532	1.0400	0.9763	0.8586	0.4778					
5		1.1497	1.2151	1.1596	1.1871	1.1504	1.1050	1.0798	1.0913	0.9638	0.7495	0.4411				
6		1.1330	1.1475	1.2354	1.2142	0.9180	1.2056	1.2116	1.1580	0.9943	0.7762	0.7503	0.4795	0.3214		
7		0.8425	1.1587	1.2010	1.0370	0.8572	1.1717	1.2309	1.1316	0.8929	0.9931	0.9644	0.8580	0.4548		
8		1.0404	1.2363	1.2018	1.0807	1.0333	1.1878	1.1523	1.1247	1.1317	1.1584	1.0915	0.9767	0.7897	0.4652	
9		1.1797	1.1413	1.1881	1.1928	1.1843	1.1712	1.1404	1.1507	1.2292	1.2109	1.0771	1.0397	0.9984	0.7063	0.3727
10		1.1162	1.1688	1.1352	1.2203	1.1254	1.1245	1.1709	1.1877	1.1705	1.2050	1.1045	1.0521	1.0301	0.8992	0.4315
11		0.8213	1.1162	1.1817	1.0031	0.8373	1.1241	1.1843	1.0356	0.8578	0.9158	1.1480	0.8805	1.0015	0.9705	0.4791
12		1.0050	1.1798	1.1301	0.8332	1.0033	1.2199	1.1909	1.0798	1.0375	1.2139	1.1859	1.1236	1.1138	1.0146	0.5402
13		1.1784	1.1841	1.1385	1.1268	1.1815	1.1347	1.1861	1.1995	1.1993	1.2356	1.1608	1.1640	1.1037	0.9779	0.5400
14		1.1179	1.1627	1.1849	1.1797	1.1187	1.1683	1.1371	1.2338	1.1572	1.1496	1.2150	1.1287	1.1195	1.0303	0.5448
15		0.8110	1.1195	1.1794	1.0030	0.8212	1.1146	1.1769	1.0356	0.8456	1.1353	1.1494	0.8503	0.9898	1.0132	0.5190

Figure 6-4. Relative Cycle Energy by Bundle – L1C9

J=	I=	16	17	18	19	20	21	22	23	24	25	26	27	28	29	30
1		0.5113	0.5058	0.4860	0.4760	0.4452	0.3909	0.3171								
2		1.0177	1.0261	0.8788	0.9917	0.9253	0.8422	0.5657	0.4116							
3		0.9930	1.1266	1.1328	1.1338	0.9605	0.9956	0.9837	0.7417	0.4605	0.3188					
4		1.1640	1.0898	1.2063	1.0556	0.8869	1.0163	1.0737	1.0541	0.8807	0.4565					
5		1.2502	1.2212	1.1210	1.2460	1.1987	1.1843	1.0462	1.0978	0.9647	0.7816	0.4507				
6		1.0836	1.0962	1.2301	1.2370	1.1080	1.1061	1.1755	1.1232	0.9551	1.0039	0.7430	0.4558	0.3229		
7		0.7884	1.0929	1.2384	1.0127	0.8794	1.2254	1.1963	0.9722	0.7845	0.9568	0.9664	0.8916	0.4736		
8		0.9364	1.2214	1.2587	1.1144	1.0125	1.2310	1.0930	0.8427	0.9746	1.1299	1.1087	1.0765	0.7922	0.4491	
9		1.2048	1.2220	1.1136	1.2575	1.2392	1.2258	1.2317	1.0953	1.2006	1.1842	1.0580	1.1005	1.0326	0.7395	0.3575
10		1.0735	1.1945	1.1024	1.2155	1.0922	1.1015	1.2277	1.2341	1.2307	1.1120	1.1979	1.0345	1.0308	0.8927	0.4168
11		0.7969	1.2038	1.2002	0.9306	0.8126	1.0934	1.2408	1.0169	0.8844	1.1144	1.2112	0.8991	0.9785	0.9540	0.4612
12		0.9677	1.2007	1.1117	0.8095	0.9321	1.2172	1.2590	1.1198	1.0180	1.2444	1.2563	1.0654	1.1494	1.0093	0.4866
13		1.1894	1.1769	1.0707	1.1117	1.2005	1.1028	1.1153	1.2617	1.2436	1.2370	1.1336	1.2167	1.1448	0.8901	0.4945
14		1.0603	1.1793	1.1767	1.1986	1.2026	1.1950	1.2242	1.2241	1.0960	1.1006	1.2276	1.0957	1.1359	1.0363	0.5346
15		0.8440	1.0594	1.1891	0.9620	0.7950	1.0725	1.2051	0.9370	0.7901	1.0858	1.2544	1.1694	0.9972	1.0227	0.5085

Figure 6-5. Relative Cycle Energy by Bundle – L1C10

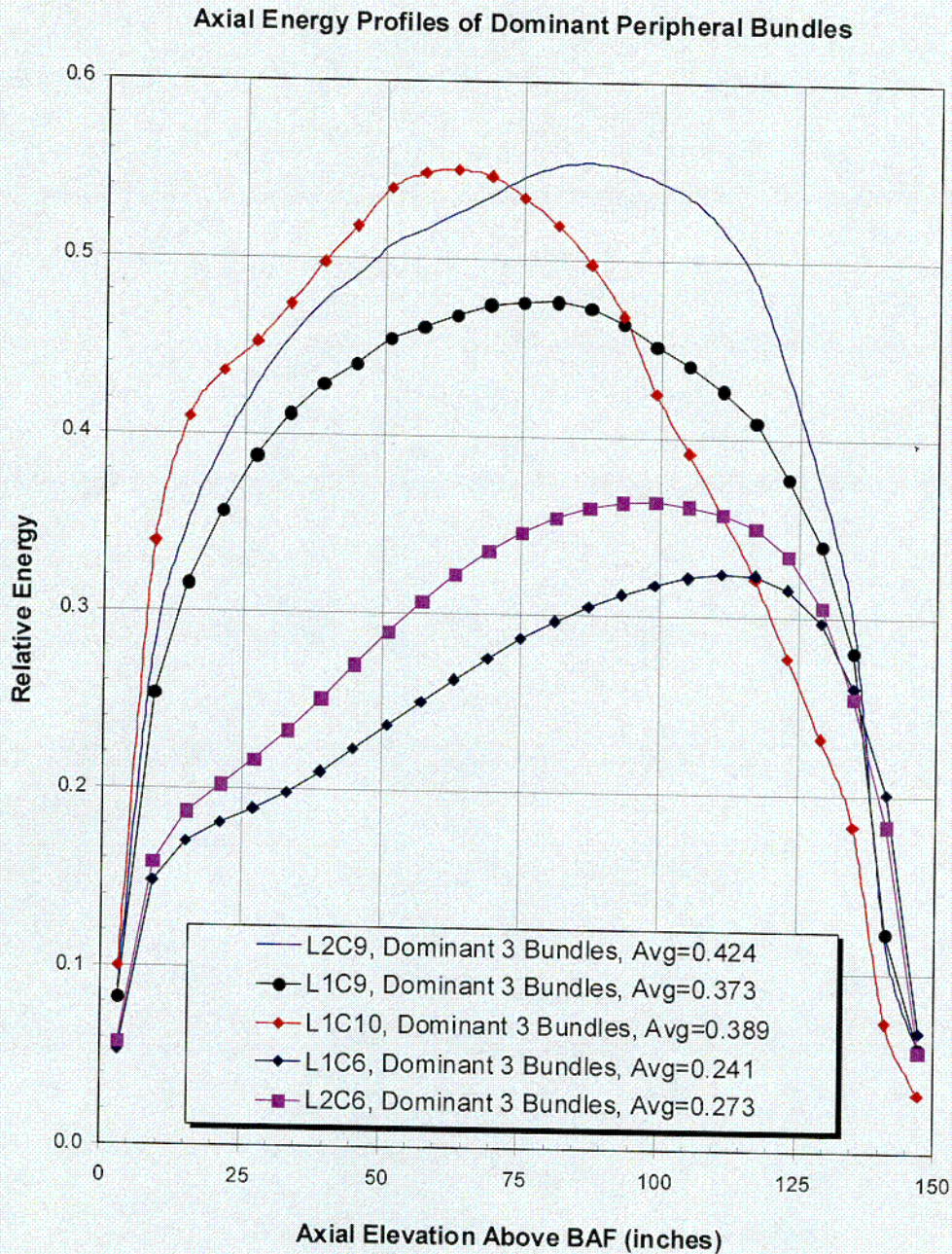
J=	I=	16	17	18	19	20	21	22	23	24	25	26	27	28	29	30
1		0.5818	0.5901	0.5837	0.5673	0.5362	0.4655	0.3088								
2		0.8518	0.9024	0.8820	0.8859	0.8285	0.7558	0.5962	0.3916							
3		1.0163	1.0455	1.0758	1.0391	1.0249	0.8864	0.8514	0.6840	0.4137	0.2757					
4		0.9989	1.1547	1.0993	1.1594	1.0676	1.0867	0.9522	0.9029	0.7142	0.3933					
5		1.2000	1.0633	1.1804	1.0785	1.1932	1.0584	1.1202	1.0185	0.9081	0.7001	0.4014				
6		1.1060	1.2056	1.0886	1.2221	1.1146	1.2112	1.1020	1.1273	0.9397	0.8542	0.7039	0.4417	0.2913		
7		1.2263	1.1210	1.2441	1.0547	1.1646	1.1055	1.2202	1.0789	1.1198	0.9383	0.9094	0.7186	0.4138		
8		1.1084	1.2556	1.1711	1.1504	1.0833	1.2356	1.1294	1.2202	1.0763	1.1240	1.0157	0.9006	0.6802	0.3692	
9		1.2592	1.0772	1.1588	1.1191	1.2404	1.0690	1.1765	1.1248	1.2159	1.0912	1.1144	0.9440	0.8454	0.5902	0.3045
10		1.1308	1.1867	1.0868	1.2180	1.1411	1.1831	1.0672	1.2317	1.1004	1.2051	1.0507	1.0798	0.8805	0.7494	0.4613
11		1.1928	1.1358	1.2518	1.0704	1.1802	1.1377	1.2372	1.0754	1.1598	1.1074	1.1869	1.0585	1.0177	0.8206	0.5306
12		1.0819	1.2595	1.1356	1.1868	1.0699	1.2158	1.1167	1.1454	1.0509	1.2186	1.0732	1.1526	1.0317	0.8779	0.5617
13		1.2553	1.1215	1.2336	1.1355	1.2509	1.0844	1.1552	1.1574	1.2409	1.0971	1.1773	1.0890	1.0681	0.8668	0.5774
14		1.1108	1.2187	1.1217	1.2594	1.1359	1.1854	1.0757	1.2523	1.1184	1.2045	1.0610	1.1500	1.0397	0.8957	0.5846
15		1.0805	1.1110	1.2556	1.0818	1.1927	1.1305	1.2582	1.1070	1.2252	1.1042	1.1982	0.9952	1.0125	0.8464	0.5781

Figure 6-6. Relative Cycle Energy by Bundle – L1C6

J=	I= 16	17	18	19	20	21	22	23	24	25	26	27	28	29	30
1	0.3265	0.3373	0.3300	0.3061	0.2855	0.2506	0.2027								
2	0.5377	0.5733	0.5780	0.5457	0.5050	0.4648	0.3806	0.2692							
3	0.8719	0.8957	0.9824	0.9411	0.7545	0.8255	0.6188	0.4814	0.3180	0.2126					
4	1.1414	1.2604	1.2617	1.1588	1.1858	1.0463	0.9648	0.8085	0.5094	0.3181					
5	1.1293	1.3501	1.1250	1.3483	1.1151	1.2723	1.0989	0.9808	0.6655	0.4730	0.2935				
6	1.3456	1.1638	1.3938	1.2580	1.3720	1.0867	1.3142	1.1994	0.8348	0.6072	0.4729	0.3179	0.2106		
7	1.0375	1.3945	1.1683	1.0953	1.2011	1.3858	1.2576	1.1669	1.0390	0.8359	0.6655	0.5093	0.3178		
8	1.1504	1.2948	1.4227	1.1303	1.1067	1.2921	1.4024	1.1022	1.1681	1.2003	0.9812	0.8081	0.4813	0.2690	
9	1.1752	1.4458	1.1833	1.4242	1.3229	1.4576	1.1645	1.4013	1.2575	1.3148	1.0974	0.9644	0.6184	0.3804	0.2027
10	1.4482	1.1717	1.4332	1.3093	1.4113	1.1738	1.4589	1.2930	1.3856	1.0861	1.2729	1.0463	0.8237	0.4646	0.2505
11	1.2038	1.4301	1.2903	0.9462	1.0621	1.4121	1.3231	1.1066	1.2011	1.3732	1.1142	1.1866	0.7541	0.5048	0.2857
12	1.0577	1.3046	1.3934	0.9510	0.9474	1.3099	1.4244	1.1297	1.0955	1.2591	1.3483	1.1583	0.9409	0.5453	0.3060
13	1.3180	1.4605	1.1699	1.3940	1.2918	1.4324	1.1815	1.4225	1.1686	1.3943	1.1242	1.2614	0.9818	0.5775	0.3298
14	1.4266	1.1749	1.4607	1.3047	1.4302	1.1754	1.4452	1.2961	1.3954	1.1650	1.3526	1.2607	0.8947	0.5731	0.3371
15	1.0633	1.4267	1.3181	1.0580	1.2049	1.4495	1.1775	1.1513	1.0382	1.3465	1.1303	1.1404	0.8724	0.5374	0.3264

Figure 6-7. Relative Cycle Energy by Bundle – L2C6

J=	I= 16	17	18	19	20	21	22	23	24	25	26	27	28	29	30
1	0.4902	0.4836	0.4718	0.4392	0.3735	0.2988	0.2274								
2	0.8784	0.9033	0.8686	0.8182	0.7360	0.5424	0.4203	0.2921							
3	1.0541	1.1583	1.1545	1.0156	0.8158	0.9511	0.6543	0.5044	0.3452	0.2232					
4	0.9413	0.9779	1.2403	0.9637	1.1004	1.1655	1.0475	0.8332	0.6400	0.3278					
5	1.2166	1.3242	1.0310	1.3037	1.2899	1.2713	0.9265	1.0026	0.6641	0.4618	0.3000				
6	1.4089	1.1289	1.3421	1.2955	0.9924	1.1780	1.2823	1.1878	0.9150	0.5998	0.4617	0.3275	0.2200		
7	1.2157	1.4018	1.0590	0.8478	0.8332	1.3176	1.1992	1.1230	0.8769	0.9149	0.6638	0.6394	0.3447		
8	1.0540	1.3149	1.4022	1.0431	1.0094	1.2215	1.3533	1.0064	1.1229	1.1875	1.0022	0.8325	0.5034	0.2905	
9	1.2837	1.4563	1.3243	1.4118	1.2940	1.3996	1.0658	1.3533	1.1990	1.2819	0.9260	1.0464	0.6528	0.4116	0.2296
10	1.3734	1.1319	1.4362	1.1291	1.3972	1.0900	1.3995	1.2214	1.3174	1.1777	1.2707	1.1646	0.9497	0.5410	0.2980
11	0.8357	1.3410	1.2704	1.2054	1.0253	1.3971	1.2939	1.0092	0.8329	0.9919	1.2894	1.0997	0.8151	0.7351	0.3729
12	0.9304	1.0516	1.3567	1.0136	1.2053	1.1289	1.4117	1.0429	0.8475	1.2951	1.3033	0.9633	1.0151	0.8177	0.4387
13	1.1864	1.3386	1.0805	1.3567	1.2703	1.4361	1.3241	1.4020	1.0588	1.3417	1.0307	1.2399	1.1540	0.8682	0.4710
14	1.3371	1.0731	1.3386	1.0515	1.3409	1.1317	1.4562	1.3147	1.4015	1.1286	1.3238	0.9775	1.1579	0.9030	0.4833
15	0.9779	1.3371	1.1864	0.9303	0.8356	1.3733	1.2836	1.0538	1.2155	1.4086	1.2163	0.9409	1.0538	0.8781	0.4899

Figure 6-8. Axial Energy Profiles of the Three Dominant Bundles

7.0 NEUTRON FLUENCE

A conservative estimation of neutron fluences at plant life of 20 and 32 EFPY can be obtained by multiplying the bounding fluxes with the EFPY. For LaSalle 1, the bounding peak RPV flux is $1.01\text{E}9 \text{ n/cm}^2\text{-s}$ and the capsule flux is $1.02\text{E}9 \text{ n/cm}^2\text{-s}$. For LaSalle 2, the bounding peak RPV flux is $1.08\text{E}9 \text{ n/cm}^2\text{-s}$ and the capsule flux is $1.07\text{E}9 \text{ n/cm}^2\text{-s}$. The bounding peak shroud flux is $2.90\text{E}12 \text{ n/cm}^2\text{-s}$ and the peak flux for the H4 weld is $2.79\text{E}12 \text{ n/cm}^2\text{-s}$ for both units. Based on these flux values, the 20-EFPY and 32-EFPY fluences are calculated, as summarized below:

	Peak RPV	Capsule	Peak Shroud	H4 Weld
LaSalle 1				
Fast Flux, $\text{n/cm}^2\text{-s}$	1.01E9	1.02E9	2.90E12	2.79E12
20-EFPY Fluence, n/cm^2	6.37E17	6.44E17	1.83E21	1.76E21
32-EFPY Fluence, n/cm^2	1.02E18	1.03E18	2.93E21	2.82E21
LaSalle 2				
Fast Flux, $\text{n/cm}^2\text{-s}$	1.08E9	1.07E9	2.90E12	2.79E12
20-EFPY Fluence, n/cm^2	6.82E17	6.75E17	1.83E21	1.76E21
32-EFPY Fluence, n/cm^2	1.09E18	1.08E18	2.93E21	2.82E21

8.0 REFERENCES

1. NEDO-32983-A, Rev. 0, "Licensing Topical Report, General Electric Methodology for Reactor Pressure Vessel Fast Neutron Flux Evaluations," December 2001.
2. Letter, S. A. Richards (USNRC) to J. F. Klapproth, "Safety Evaluation for NEDC-32983P, General Electric Methodology for Reactor Pressure Vessel Fast Neutron Flux Evaluation (TAC No. MA9891)," MFN 01-050, September 14, 2001.
3. Regulatory Guide 1.190, "Calculational and Dosimetry Methods for Determining Pressure Vessel Neutron Fluence," U.S. NRC, March 2001.
4. CCC-543, "TORT-DORT Two- and Three-Dimensional Discrete Ordinates Transport Version 2.8.14," Radiation Shielding Information Center (RSIC), January 1994.
5. A. S. Pallota (Exelon), "L1C9/L2C9 Data Requested by GE for Flux Evaluations," NFM0200054, Sequence 0, dated 03/08/2002.
6. J. M. Shields (Exelon), "LaSalle Unit 1 and Unit 2 Flux Data," SEAG 02-000069 dated 3/22/2002.
7. Letter, S. A. Richards (USNRC) to G. A. Watford, "Amendment 26 to GE Licensing Topical Report NEDE-24011-P-A, GESTAR II – Implementing Improved GE Steady-State Methods (TAC No. MA6481)," November 10, 1999.
8. A. S. Pallota (Exelon), "L1C10 Data Requested by GE for Flux Evaluations," NFM0200002, Sequence 0, dated 01/04/2002.
9. A. S. Pallota (Exelon), "L1C6/L2C6 Data Requested by GE for Flux Evaluations," NFM0200055, Sequence 0, dated 03/08/2002.

APPENDIX A PLOT DATA

(a) Flux Distribution

Azimuth (degrees)				Elevation Above BAF		
	Fig. 4-1	Fig. 4-3	Fig. 5-1	(Inches)	Fig. 4-2	Fig. 4-4
0.125	4.04E+08	3.76E+11	3.80E+08	-29.49	2.04E-03	2.45E-05
0.5	4.03E+08	3.74E+11	3.80E+08	-28.48	2.79E-03	3.44E-05
1	4.04E+08	3.77E+11	3.81E+08	-27.47	3.46E-03	4.64E-05
1.5	4.06E+08	3.78E+11	3.82E+08	-26.46	4.23E-03	6.07E-05
2	4.09E+08	3.81E+11	3.85E+08	-25.45	5.10E-03	7.96E-05
2.5	4.12E+08	3.85E+11	3.88E+08	-24.44	6.12E-03	1.04E-04
3	4.16E+08	3.90E+11	3.92E+08	-23.44	7.29E-03	1.35E-04
3.5	4.21E+08	3.97E+11	3.97E+08	-22.45	8.65E-03	1.77E-04
4	4.27E+08	4.02E+11	4.02E+08	-21.45	1.02E-02	2.31E-04
4.5	4.33E+08	4.11E+11	4.08E+08	-20.45	1.21E-02	3.03E-04
5	4.41E+08	4.20E+11	4.15E+08	-19.45	1.42E-02	3.99E-04
5.5	4.49E+08	4.30E+11	4.23E+08	-18.46	1.67E-02	5.23E-04
6	4.58E+08	4.41E+11	4.32E+08	-17.46	1.95E-02	6.92E-04
6.5	4.68E+08	4.54E+11	4.41E+08	-16.46	2.27E-02	9.09E-04
7	4.79E+08	4.66E+11	4.51E+08	-15.46	2.64E-02	1.21E-03
7.5	4.92E+08	4.83E+11	4.63E+08	-14.47	3.06E-02	1.59E-03
8	5.04E+08	4.98E+11	4.74E+08	-13.47	3.53E-02	2.11E-03
8.5	5.19E+08	5.18E+11	4.88E+08	-12.47	4.05E-02	2.80E-03
9	5.33E+08	5.36E+11	5.02E+08	-11.47	4.64E-02	3.72E-03
9.5	5.50E+08	5.59E+11	5.18E+08	-10.48	5.30E-02	4.93E-03
10	5.66E+08	5.83E+11	5.33E+08	-9.48	6.04E-02	6.53E-03
10.5	5.85E+08	6.08E+11	5.50E+08	-8.48	6.86E-02	8.67E-03
11	6.03E+08	6.37E+11	5.68E+08	-7.48	7.77E-02	1.15E-02
11.5	6.23E+08	6.66E+11	5.87E+08	-6.48	8.78E-02	1.52E-02
12	6.44E+08	7.01E+11	6.06E+08	-5.49	9.89E-02	2.03E-02
12.5	6.66E+08	7.36E+11	6.27E+08	-4.49	1.11E-01	2.71E-02
13	6.89E+08	7.76E+11	6.48E+08	-3.49	1.24E-01	3.57E-02
13.5	7.12E+08	8.19E+11	6.69E+08	-2.49	1.38E-01	4.68E-02
14	7.36E+08	8.66E+11	6.92E+08	-1.50	1.53E-01	6.08E-02
14.5	7.61E+08	9.16E+11	7.15E+08	-0.50	1.69E-01	7.92E-02
15	7.85E+08	9.71E+11	7.38E+08	0.75	0.188	0.105
15.5	8.11E+08	1.03E+12	7.61E+08	2.25	0.214	0.142

16	8.34E+08	1.10E+12	7.83E+08	3.75	0.241	0.182
16.5	8.57E+08	1.17E+12	8.05E+08	5.25	0.270	0.226
17	8.79E+08	1.25E+12	8.25E+08	6.75	0.299	0.281
17.5	9.00E+08	1.34E+12	8.45E+08	8.25	0.328	0.329
18	9.19E+08	1.43E+12	8.63E+08	9.75	0.358	0.368
18.5	9.37E+08	1.53E+12	8.79E+08	11.25	0.387	0.402
19	9.50E+08	1.64E+12	8.91E+08	12.60	0.413	0.432
19.5	9.59E+08	1.76E+12	8.99E+08	13.80	0.436	0.454
20	9.61E+08	1.89E+12	9.02E+08	15.00	0.458	0.473
20.5	9.67E+08	2.02E+12	9.08E+08	16.20	0.478	0.489
21	9.71E+08	2.16E+12	9.12E+08	17.40	0.498	0.505
21.5	9.78E+08	2.31E+12	9.19E+08	18.60	0.517	0.521
22	9.83E+08	2.46E+12	9.24E+08	19.80	0.535	0.535
22.5	9.92E+08	2.59E+12	9.32E+08	21.00	0.552	0.547
23	1.00E+09	2.71E+12	9.43E+08	22.20	0.569	0.558
23.5	1.02E+09	2.82E+12	9.56E+08	23.40	0.584	0.570
24	1.03E+09	2.88E+12	9.68E+08	24.50	0.598	0.581
24.5	1.04E+09	2.90E+12	9.79E+08	25.50	0.610	0.590
25	1.06E+09	2.82E+12	9.92E+08	26.50	0.622	0.599
25.5	1.07E+09	2.64E+12	1.00E+09	27.50	0.633	0.607
26	1.08E+09	2.45E+12	1.01E+09	28.50	0.644	0.615
26.5	1.07E+09	2.29E+12	1.01E+09	29.50	0.654	0.623
27	1.06E+09	2.13E+12	9.96E+08	30.50	0.665	0.632
27.5	1.05E+09	2.01E+12	9.79E+08	31.50	0.674	0.640
28	1.01E+09	1.90E+12	9.49E+08	32.50	0.684	0.648
28.5	9.37E+08	1.79E+12	8.77E+08	33.50	0.693	0.655
29	9.00E+08	1.70E+12	8.41E+08	34.50	0.702	0.662
29.5	8.79E+08	1.62E+12	8.20E+08	35.50	0.710	0.670
30	8.60E+08	1.54E+12	8.02E+08	36.50	0.719	0.678
30.5	8.45E+08	1.47E+12	7.88E+08	37.50	0.727	0.685
31	8.30E+08	1.40E+12	7.75E+08	38.50	0.735	0.692
31.5	8.27E+08	1.36E+12	7.75E+08	39.50	0.743	0.699
32	8.62E+08	1.32E+12	8.06E+08	40.50	0.750	0.706
32.5	8.67E+08	1.31E+12	8.13E+08	41.50	0.758	0.713
33	8.60E+08	1.30E+12	8.06E+08	42.43	0.765	0.720
33.5	8.51E+08	1.32E+12	7.99E+08	43.29	0.771	0.726
34	8.40E+08	1.34E+12	7.88E+08	44.14	0.778	0.732
34.5	8.24E+08	1.38E+12	7.73E+08	45.00	0.783	0.738
35	8.04E+08	1.42E+12	7.54E+08	45.86	0.790	0.744
35.5	7.82E+08	1.46E+12	7.34E+08	46.71	0.795	0.750
36	7.62E+08	1.50E+12	7.16E+08	47.57	0.802	0.757

36.5	7.42E+08	1.53E+12	6.97E+08	48.43	0.807	0.764
37	7.23E+08	1.55E+12	6.80E+08	49.29	0.813	0.771
37.5	7.08E+08	1.54E+12	6.66E+08	50.14	0.819	0.777
38	6.98E+08	1.47E+12	6.57E+08	51.00	0.825	0.782
38.5	6.91E+08	1.38E+12	6.49E+08	51.86	0.830	0.788
39	6.87E+08	1.28E+12	6.46E+08	52.71	0.836	0.793
39.5	6.86E+08	1.18E+12	6.44E+08	53.57	0.841	0.799
40	6.87E+08	1.08E+12	6.46E+08	54.43	0.847	0.805
40.5	6.89E+08	9.91E+11	6.48E+08	55.29	0.852	0.811
41	6.88E+08	9.09E+11	6.47E+08	56.14	0.857	0.817
41.5	6.84E+08	8.43E+11	6.43E+08	57.00	0.862	0.822
42	6.79E+08	7.82E+11	6.39E+08	57.86	0.868	0.827
42.5	6.73E+08	7.35E+11	6.33E+08	58.71	0.873	0.832
43	6.68E+08	6.97E+11	6.28E+08	59.57	0.878	0.838
43.5	6.63E+08	6.71E+11	6.24E+08	60.38	0.882	0.843
44	6.60E+08	6.53E+11	6.20E+08	61.13	0.887	0.848
44.5	6.58E+08	6.41E+11	6.19E+08	61.88	0.891	0.853
45	6.57E+08	6.37E+11	6.18E+08	62.63	0.895	0.858
45.5	6.58E+08	6.41E+11	6.19E+08	63.38	0.900	0.862
46	6.60E+08	6.53E+11	6.20E+08	64.13	0.904	0.867
46.5	6.63E+08	6.71E+11	6.24E+08	64.88	0.908	0.871
47	6.68E+08	6.97E+11	6.28E+08	65.63	0.912	0.876
47.5	6.73E+08	7.35E+11	6.33E+08	66.38	0.916	0.881
48	6.79E+08	7.82E+11	6.39E+08	67.13	0.920	0.886
48.5	6.84E+08	8.43E+11	6.43E+08	67.88	0.924	0.891
49	6.88E+08	9.09E+11	6.47E+08	68.63	0.928	0.895
49.5	6.89E+08	9.90E+11	6.47E+08	69.38	0.932	0.900
50	6.87E+08	1.08E+12	6.46E+08	70.13	0.935	0.904
50.5	6.85E+08	1.18E+12	6.44E+08	70.88	0.939	0.909
51	6.87E+08	1.28E+12	6.46E+08	71.63	0.943	0.914
51.5	6.91E+08	1.38E+12	6.49E+08	72.33	0.946	0.918
52	6.97E+08	1.47E+12	6.56E+08	73.00	0.949	0.922
52.5	7.08E+08	1.54E+12	6.66E+08	73.67	0.952	0.926
53	7.23E+08	1.55E+12	6.80E+08	74.33	0.955	0.930
53.5	7.42E+08	1.53E+12	6.97E+08	75.00	0.958	0.934
54	7.61E+08	1.50E+12	7.15E+08	75.67	0.961	0.937
54.5	7.82E+08	1.46E+12	7.34E+08	76.33	0.964	0.941
55	8.03E+08	1.42E+12	7.54E+08	77.00	0.966	0.944
55.5	8.23E+08	1.38E+12	7.72E+08	77.67	0.969	0.948
56	8.38E+08	1.34E+12	7.86E+08	78.38	0.971	0.952
56.5	8.48E+08	1.32E+12	7.96E+08	79.13	0.974	0.956

57	8.54E+08	1.30E+12	8.02E+08	79.88	0.977	0.959
57.5	8.60E+08	1.30E+12	8.08E+08	80.63	0.979	0.963
58	8.65E+08	1.32E+12	8.13E+08	81.38	0.981	0.965
58.5	8.71E+08	1.36E+12	8.19E+08	82.13	0.984	0.969
59	8.77E+08	1.40E+12	8.24E+08	82.88	0.986	0.972
59.5	8.88E+08	1.47E+12	8.35E+08	83.63	0.988	0.975
60	9.02E+08	1.54E+12	8.48E+08	84.38	0.990	0.978
60.5	9.23E+08	1.62E+12	8.68E+08	85.13	0.991	0.980
61	9.48E+08	1.70E+12	8.91E+08	85.88	0.993	0.983
61.5	9.78E+08	1.79E+12	9.18E+08	86.63	0.994	0.985
62	1.01E+09	1.89E+12	9.47E+08	87.38	0.996	0.987
62.5	1.03E+09	2.00E+12	9.70E+08	88.13	0.997	0.989
63	1.06E+09	2.13E+12	9.90E+08	88.88	0.998	0.990
63.5	1.07E+09	2.28E+12	1.00E+09	89.63	0.998	0.992
64	1.07E+09	2.45E+12	1.01E+09	90.43	0.999	0.994
64.5	1.07E+09	2.64E+12	1.00E+09	91.29	1.000	0.995
65	1.06E+09	2.82E+12	9.91E+08	92.14	1.000	0.997
65.5	1.04E+09	2.90E+12	9.79E+08	93.00	1.000	0.998
66	1.03E+09	2.88E+12	9.67E+08	93.86	1.000	0.998
66.5	1.02E+09	2.82E+12	9.56E+08	94.71	0.999	0.999
67	1.00E+09	2.71E+12	9.43E+08	95.57	0.999	0.999
67.5	9.92E+08	2.59E+12	9.32E+08	96.43	0.998	1.000
68	9.83E+08	2.46E+12	9.23E+08	97.29	0.997	1.000
68.5	9.78E+08	2.31E+12	9.19E+08	98.14	0.995	1.000
69	9.71E+08	2.16E+12	9.11E+08	99.00	0.993	1.000
69.5	9.67E+08	2.02E+12	9.07E+08	99.86	0.991	0.999
70	9.61E+08	1.88E+12	9.02E+08	100.71	0.989	0.998
70.5	9.58E+08	1.76E+12	8.99E+08	101.57	0.986	0.998
71	9.49E+08	1.64E+12	8.91E+08	102.43	0.983	0.997
71.5	9.36E+08	1.53E+12	8.79E+08	103.29	0.979	0.995
72	9.19E+08	1.43E+12	8.62E+08	104.14	0.976	0.994
72.5	8.99E+08	1.34E+12	8.44E+08	105.00	0.972	0.991
73	8.79E+08	1.25E+12	8.25E+08	105.86	0.967	0.989
73.5	8.56E+08	1.17E+12	8.04E+08	106.71	0.962	0.986
74	8.33E+08	1.10E+12	7.82E+08	107.57	0.957	0.983
74.5	8.09E+08	1.03E+12	7.60E+08	108.50	0.950	0.979
75	7.83E+08	9.72E+11	7.37E+08	109.50	0.943	0.974
75.5	7.59E+08	9.16E+11	7.13E+08	110.50	0.935	0.969
76	7.33E+08	8.66E+11	6.89E+08	111.50	0.927	0.963
76.5	7.07E+08	8.19E+11	6.65E+08	112.50	0.917	0.957
77	6.82E+08	7.77E+11	6.42E+08	113.50	0.907	0.949

77.5	6.57E+08	7.36E+11	6.18E+08	114.50	0.896	0.940
78	6.33E+08	7.02E+11	5.96E+08	115.50	0.884	0.931
78.5	6.09E+08	6.66E+11	5.73E+08	116.50	0.871	0.921
79	5.85E+08	6.37E+11	5.50E+08	117.50	0.858	0.910
79.5	5.61E+08	6.08E+11	5.28E+08	118.50	0.844	0.897
80	5.36E+08	5.83E+11	5.05E+08	119.50	0.829	0.883
80.5	5.13E+08	5.59E+11	4.83E+08	120.50	0.813	0.867
81	4.91E+08	5.36E+11	4.62E+08	121.50	0.796	0.852
81.5	4.71E+08	5.18E+11	4.44E+08	122.50	0.778	0.835
82	4.51E+08	4.98E+11	4.25E+08	123.50	0.760	0.818
82.5	4.34E+08	4.83E+11	4.09E+08	124.50	0.741	0.800
83	4.20E+08	4.66E+11	3.96E+08	125.50	0.721	0.780
83.5	4.11E+08	4.53E+11	3.87E+08	126.60	0.698	0.756
84	4.02E+08	4.40E+11	3.79E+08	127.80	0.672	0.730
84.5	3.95E+08	4.29E+11	3.72E+08	129.00	0.645	0.703
85	3.90E+08	4.19E+11	3.67E+08	130.20	0.617	0.674
85.5	3.84E+08	4.10E+11	3.62E+08	131.40	0.588	0.641
86	3.79E+08	4.01E+11	3.57E+08	132.60	0.557	0.603
86.5	3.73E+08	3.96E+11	3.51E+08	133.80	0.526	0.565
87	3.67E+08	3.89E+11	3.45E+08	135.00	0.496	0.525
87.5	3.61E+08	3.84E+11	3.40E+08	136.20	0.465	0.481
88	3.56E+08	3.80E+11	3.35E+08	137.40	0.435	0.431
88.5	3.50E+08	3.77E+11	3.30E+08	138.75	0.401	0.370
89	3.46E+08	3.75E+11	3.26E+08	140.25	0.365	0.315
89.5	3.43E+08	3.73E+11	3.24E+08	141.75	0.329	0.268
89.875	3.44E+08	3.75E+11	3.24E+08	143.25	0.294	0.225
				144.75	0.262	0.186
				146.25	0.231	0.153
				147.75	0.204	0.124
				149.25	0.179	0.099
				150.49	1.61E-01	8.13E-02
				151.48	1.46E-01	6.95E-02
				152.46	1.33E-01	5.99E-02
				153.45	1.20E-01	5.17E-02
				154.44	1.09E-01	4.49E-02
				155.42	9.80E-02	3.90E-02
				156.41	8.82E-02	3.41E-02
				157.40	7.92E-02	2.98E-02
				158.38	7.10E-02	2.62E-02
				159.37	6.36E-02	2.30E-02
				160.35	5.69E-02	2.02E-02

161.34	5.08E-02	1.77E-02
162.33	4.54E-02	1.55E-02
163.32	4.04E-02	1.35E-02
164.33	3.60E-02	1.16E-02
165.34	3.19E-02	9.86E-03
166.36	2.83E-02	8.31E-03
167.37	2.51E-02	6.95E-03
168.38	2.22E-02	5.78E-03
169.39	1.96E-02	4.79E-03
170.40	1.73E-02	3.96E-03
171.41	1.52E-02	3.28E-03
172.42	1.34E-02	2.71E-03
173.43	1.17E-02	2.23E-03
174.44	1.02E-02	1.84E-03
175.45	8.89E-03	1.50E-03
176.46	7.67E-03	1.23E-03
177.47	6.51E-03	9.91E-04
178.48	5.41E-03	7.87E-04
179.49	4.04E-03	5.74E-04

(b) Figure 6-8

Elevation above BAF					
(inches)	L2C9	L1C9	L1C10	L1C6	L2C9
147	0.057	0.059	0.033	0.067	0.056
141	0.118	0.123	0.073	0.201	0.183
135	0.294	0.280	0.182	0.260	0.255
129	0.373	0.340	0.232	0.297	0.305
123	0.435	0.378	0.277	0.315	0.334
117	0.487	0.409	0.321	0.323	0.349
111	0.516	0.427	0.357	0.324	0.357
105	0.535	0.441	0.392	0.322	0.362
99	0.544	0.452	0.425	0.317	0.364
93	0.551	0.464	0.468	0.312	0.364
87	0.554	0.472	0.497	0.305	0.360
81	0.552	0.476	0.519	0.296	0.354
75	0.545	0.475	0.534	0.286	0.346
69	0.536	0.474	0.546	0.275	0.335
63	0.526	0.468	0.550	0.263	0.322
57	0.516	0.461	0.547	0.250	0.307
51	0.507	0.454	0.539	0.236	0.289
45	0.490	0.440	0.517	0.223	0.270
39	0.475	0.429	0.497	0.210	0.251
33	0.455	0.412	0.473	0.198	0.233
27	0.428	0.388	0.452	0.189	0.216
21	0.394	0.356	0.435	0.180	0.202
15	0.350	0.316	0.409	0.170	0.187
9	0.280	0.254	0.339	0.148	0.158
3	0.089	0.083	0.100	0.053	0.058
Avg	0.424	0.373	0.389	0.241	0.273